Title: A novel inhibitory nucleo-cortical circuit controls cerebellar Golgi cell activity

Running title: Nucleo-cortical inhibition of the cerebellar Golgi cells

Lea Ankri[1]*, Zoé Husson[2,3,4]*, Katarzyna Pietrajtis[2,3,4], Rémi Proville[3,4,5], Clément Léna[3,4,5], Yosef Yarom[1], Stéphane Dieudonné[2,3,4], Marylka Yoe Uusisaari[1]

1. Edmond and Lily Safra Center for Brain Sciences (ELSC), Department of Neurobiology, Hebrew University of Jerusalem, Israel.
2. Inhibitory Transmission Team, IBENS, Ecole Normale Supérieure, 46 rue d'Ulm, 75005 Paris, France.
3. CNRS UMR8197, Ecole Normale Supérieure, 46 rue d'Ulm, 75005 Paris, France
4. INSERM U1024, Ecole Normale Supérieure, 46 rue d'Ulm, 75005 Paris, France
5. Cerebellum Team, IBENS, Ecole Normale Supérieure, 46 rue d'Ulm, 75005 Paris, France.

Corresponding author: Stéphane Dieudonné dieudon@biologie.ens.fr

* Contributed equally to the work

IMPACT STATEMENT

The neglected glycinergic neurons of the cerebellar nuclei project extensively to the cerebellar cortex and inhibit GABAergic Golgi cells, a major source of granule cell inhibition.

ABSTRACT

The cerebellum, a crucial center for motor coordination, is composed of a cortex and several nuclei. The main mode of interaction between these two parts is considered to be formed by the inhibitory control of the nuclei by cortical Purkinje neurons. We now amend this view by showing that inhibitory GABA-glycinergic neurons of the cerebellar nuclei project profusely into the cerebellar cortex, where they make synaptic contacts on a GABAergic subpopulation of cerebellar Golgi cells. These spontaneously firing Golgi cells are inhibited by optogenetic activation of the inhibitory nucleo-cortical fibers both *in vitro* and *in vivo*. Our data suggest that the cerebellar nuclei may contribute to the functional recruitment of the cerebellar cortex by decreasing Golgi cell inhibition onto granule cells.

32
33
34 **INTRODUCTION**

35 The cerebellum plays a key role in the fine temporal control of posture and movements as well as
36 in cognitive processes (Ito, 1993; Leiner et al., 1993). Current cerebellar theories (Apps and Garwicz,
37 2005; Jacobson et al., 2008; Dean and Porrill, 2009) mainly discuss cerebellar computation from the
38 point of view of its cortical circuitry, where both pre-cerebellar mossy fibers (MFs) and inferior olive (IO)-
39 originating climbing fibers (CFs) modulate Purkinje neuron (PN) spiking. Sensory-motor signal processing
40 in the main cerebellar output structure, the cerebellar nuclei (CN), has received less attention. Modulation
41 of spike frequency and timing in the CN projection neurons is considered to be mostly determined by the
42 massive inhibitory cortico-nuclear projection of PNs (Chan-Palay, 1977; De Zeeuw and Berrebi, 1995;
43 Telgkamp and Raman, 2002; Pedroarena and Schwarz, 2003; Telgkamp et al., 2004; Person and Raman,
44 2012; Gauck and Jaeger, 2000; Najac and Raman, 2015) . However, certain aspects of cerebellar function
45 persist even when the cerebellar cortex is selectively inactivated or damaged (Thompson and Steinmetz,
46 2009; Clopath et al., 2014; Longley and Yeo, 2014; Aoki et al., 2014). Thus, a better understanding of the
47 information processing in the CN as well as its influence on cerebellar cortical computation is needed.

48 Currently, the cerebellar cortex and the CN are known to interact through two circuits. The best
49 known is the nucleo-olivary (NO) circuit (Apps and Garwicz, 2005; Apps and Hawkes, 2009; Chaumont et
50 al., 2013), where the small GABAergic CN cells, subject to PN inhibition (Najac and Raman, 2015) , project
51 to the contralateral IO (Fredette and Mugnaini, 1991) . This pathway regulates olivary activity (Chen et al.,
52 2010; Bazzigaluppi et al., 2012; Chaumont et al., 2013; Lefler et al., 2014) and thereby complex spike ac-
53 tivity in the PNs and cerebellar cortical plasticity (Hansel and Linden, 2000; Coesmans et al., 2004;
54 Bengtsson and Hesslow, 2006; Medina and Lisberger, 2008) . A less-known nucleo-cortical circuit is
55 formed by the glutamatergic neurons of the CN which, in addition to projecting to various premotor and
56 associative regions of the brain (Tsukahara and Bando, 1970; Asanuma et al., 1980; Angaut et al., 1985;
57 Sultan et al., 2012; Ruigrok and Teune, 2014) send axonal collaterals to the cerebellar granule cell layer
58 (GrCL; Houck and Person, 2015) . These collateral fibers form mossy-fiber-like terminals contacting gran-
59 ule cell (GrCs) and Golgi cell dendrites (see also Tolbert et al., 1976, 1977, 1978; Hámori et al., 1980;
60 Payne, 1983) . The functional significance of this excitatory nucleo-cortical pathway, loosely following the
61 modular arrangement of the cerebellum (Dietrichs and Walberg, 1979; Gould, 1979; Haines and Pearson,
62 1979; Tolbert and Bantli, 1979; Buisseret-Delmas, 1988; Provini et al., 1998; Ruigrok, 2010 ; reviewed by

63 Houck and Person, 2013), is likely related to efference copying of motor commands to the cerebellar cor-
64 tex (Sommer and Wurtz, 2008; Houck and Person, 2015).

65 In addition to the pathways linking the CN with the cerebellar cortex mentioned above, evidence
66 has occasionally emerged for an inhibitory nucleo-cortical (iNC) pathway. GABAergic neurons have been
67 shown to be labeled in the CN by retrograde tracing from the cerebellar cortex (Batini et al., 1989) and
68 nucleo-cortical terminals with non-glutamatergic ultrastructural features have been found to contact pu-
69 tative Golgi cell dendrites (Tolbert et al., 1980) . More recently, it was demonstrated that GlyT2-
70 expressing CN neurons extend axons toward the cerebellar cortex (Uusisaari and Knöpfel, 2010) , suggest-
71 ing that the iNC pathway might be identifiable by its glycinergic phenotype. While the iNC projection is
72 likely to have significant impact on cerebellar computation, its postsynaptic targets and its functional or-
73 ganization remain unknown.

74 To establish the existence and prevalence of an inhibitory connection between the CN and the
75 cerebellar cortex, we employed specific viral targeting of GABAergic and glycinergic neurons in the CN of
76 GAD-cre and GlyT2-cre transgenic mouse lines, respectively (Taniguchi et al., 2011; Husson et al., 2014) .
77 We found that the GABA-glycinergic CN neurons form an extensive plexus of iNC axons, which contact
78 Golgi cells in the cerebellar granular and molecular layers. Specific optogenetic activation of the iNC axons
79 inhibited spikes in a distinct subpopulation of Golgi cells, characterized by their spontaneous firing, high
80 neurogranin immunoreactivity and negligible GlyT2 expression. As the functional significance of the iNC
81 pathway is likely to be amplified by the high divergence of Golgi cells, which target thousands of GrCs
82 (Hámori and Somogyi, 1983; Jakab and Hamori, 1988; Andersen et al., 1992; Korbo et al., 1993) , as well as
83 the remarkable mediolateral extent of the iNC axons, the CN might play a key role in the regulation of the
84 information flow through the GrCL.
85

86 **RESULTS**

87 **Nucleo-cortical projection neurons have a mixed GABA-glycine phenotype**

88 In order to identify the inhibitory nucleo-cortical projection neurons, we specifically labeled the
89 GABAergic and glycinergic cerebellar nuclei (CN) neurons by injecting floxed adeno-associated virus
90 (AAV) in the CN of GAD-cre and GlyT2-cre transgenic mouse lines, respectively. As shown in Figure 1 (A1
91 and B1), these procedures resulted in the expression of the fluorophores (mCherry in GAD-cre and YFP in
92 GlyT2-cre mice) in a subset of CN neurons. In the GAD-cre mice, the labeled neurons displayed a wide
93 range of sizes and shapes, including both globular and multipolar morphologies (Figure 1A2, arrow and
94 arrowhead, respectively). In contrast, in GlyT2-cre mice, the labeled neurons were predominantly large
95 (Figure 1B2, arrowhead) and multipolar, often with a thick principal dendrite (Figure 1B2, arrows). To
96 examine the morphological difference between CN cells labeled in GAD-cre and GlyT2-cre mice, we
97 measured and compared their soma sizes. The size distribution in GAD-cre CN was best fitted with a two-
98 component Gaussian model (Figure 1D, red bars and line; Gaussian peaks at 11.9 μm and 16.2 μm; R-
99 square 0.97, n = 650 cells in 6 animals), suggesting it is composed of two separate populations. In contrast,
100 the optimal fit to the size distribution of GlyT2-cre neurons was obtained with a single-component
101 Gaussian model (Figure 1D, yellow bars and line; peak at 16.6 μm, R-square = 0.83, n = 118 cells in 4
102 animals; KS-test GAD vs. GlyT2, $p < 0.0001$). The peak of this GlyT2-fit matched well with the right-most
103 peak in the GAD-cre distribution (GAD-cre, second peak confidence interval, 13.6 - 18.8 μm; GlyT2-cre
104 confidence interval, 16.0 - 17.1 μm).

105 The difference between the GAD-cre and GlyT2-cre populations, corresponding to the left-most
106 peak in the GAD-cre distribution (Figure 1D), likely corresponds to the nucleo-olivary (NO) cells that are
107 also transfected in the GAD-cre model, as evidenced by the presence of fluorescent axons in the inferior
108 olive (IO; Figure 1A3; see Lefler et al., 2014). To confirm this, we retrogradely labeled the NO cells via viral
109 injections in the IO (Figure 1C). The size distribution of the NO neurons (mean: 12.8 ± 2.4 μm; n = 193
110 cells in 4 animals; see also Najac and Raman, 2015) was significantly different from the GlyT2 cells (NO vs.
111 GlyT2 KS-test, $p < 0.0001$, Figure 1D). Furthermore, the NO size distribution was well fitted with a single
112 Gaussian with a peak closely resembling the left-most peak of the GAD-cre distribution (Figure 1D, green
113 bars and line; peak at 12.3 μm, confidence interval 12.0 - 12.7 μm; R-square 0.93; n = 193 cells in 4
114 animals). Thus, we conclude that the mixed GABA-glycinergic neurons form a separate population from
115 the purely GABAergic NO neurons that are not transfected in adult GlyT2-cre animals (Husson et al.,

116 2014). These glycinergic neurons, like all other CN neurons, receive functional inputs from PN axons
117 (Figure 1 –figure supplement 1), as previously suggested by immunohistochemical and optogenetic
118 studies (De Zeeuw and Berrebi, 1995; Teune et al., 1998).

119 In contrast to the NO axons, which leave the CN towards the brainstem, we found that axons of
120 the large multipolar GAD and GlyT2-positive neurons projected across the white matter surrounding the
121 CN and into the cerebellar cortex (as shown in Figure 1E1 and E2 for the GAD-cre and GlyT2-cre cerebella,
122 respectively). In the vermis, the projections regularly crossed the midline and extended into the
123 contralateral cortex, but otherwise the projection was predominantly ipsilateral. The divergence of
124 nucleo-cortical axons in the cortex varied depending on the extent and localization of viral transfection,
125 coarsely following the known cerebellar modules (Pijpers et al., 2005 ; Apps and Garwicz, 2005; Apps and
126 Hawkes, 2009) . Lateral CN injections labeled axons in the lateral and intermediate hemispheres and the
127 flocculi (Figure 1F1) whereas medial CN injections yielded labeled axons predominantly in the vermal
128 cerebellum (Figure 1F2). Surprisingly, individual nucleo-cortical axons could be seen to travel long
129 distances in the medio-lateral direction (up to several millimeters; see inset in Figure 1F2) forming
130 boutons within the granule cell layer (GrCL).

131 The nucleo-cortical axons formed dense meshes in the GrCL (Figures 2A1, B1). As seen in high
132 magnification images (Figures 2A2, B2), the axons formed large swellings that were also seen in the
133 molecular layer (ML; Figures 2A3, B3). The axons in the two cre lines were remarkably similar in their
134 appearance, even though the swellings labeled with mCherry in the GAD-cre line appeared nearly identical
135 to the varicosities labeled by YFP in the GlyT2-cre line (Figures 2A2, B2, C1; cross-sectional areas in GAD-
136 cre, red bars, 2.1 ± 0.9 μm^2, n = 400 varicosities; in GlyT2-cre, yellow bars, 1.87 ± 0.9 μm^2, n = 415
137 varicosities; KS-test, p = 0.013). Also, no large differences were evident among boutons found in the GrCL
138 or ML (Figure 2C2; KS-test, p = 0.023). These anatomical similarities imply that the axons labeled in the
139 two transfection models represent the projections of a specific population of CN neurons with a mixed
140 GABA-glycinergic phenotype (Husson et al., 2014). Indeed, immunostaining revealed that virtually all the
141 nucleo-cortical fibers in the GAD-cre transfected mice were immunoreactive for GlyT2 (Figure 2D1-2; 94.6
142 ± 6.2 %, n = 2 animals, n = 9 stacks, n = 422 varicosities; Figure 2D) while those in GlyT2-cre cerebella
143 were reactive for GAD65-67 (93.9 ± 5.0 %, n = 3 animals, n = 7 stacks, n = 565 varicosities; Figure 2E1-2).
144 These results unequivocally demonstrate the dual neurotransmitter phenotype of the nucleo-cortical
145 projection. Notably, neither rosette-like terminals nor evidence of contacts within cerebellar glomeruli

146 were found. This indicates that they differ both in shape and location from the excitatory MFs and the
147 glutamatergic nucleo-cortical fibers described earlier in the literature, both forming rosette-like terminals
148 within the glomeruli (Tolbert et al., 1978; Hámori et al., 1980; Batini et al., 1992; Houck and Person,
149 2015) .

150 **Nucleo-cortical fibers inhibit Golgi cell activity**

151 Having demonstrated the existence of a GABA-glycinergic projection from the CN to the cerebellar
152 cortex, generated by a distinct cell type of the CN, we proceeded to identify the targets of this inhibitory
153 nucleo-cortical (iNC) pathway. Golgi cells, which are the only ubiquitous cerebellar neurons that express
154 glycine receptors in the cerebellar cortex (Dieudonné, 1995) , as well as the only neurons with dendrites
155 both in the granular and molecular layers, constitute the most likely targets for iNC axons. To investigate
156 this possibility, we introduced a non-specific GFP-expressing virus to the cerebellar cortex of GAD-cre
157 mice transfected as above in the CN, to be able to visualize neurons in the GrCL. This procedure labeled
158 Golgi cells and indeed we found axonal swellings of iNC fibers apposed along the proximal dendrites and
159 cell bodies of Golgi cells (Figure 3A, arrows).

160 To physiologically confirm the presence of functional inhibitory synaptic connections between
161 the CN and the cerebellar cortex, we selectively activated channelrhodopsin (ChR2) in the iNC axons with
162 single, 5 ms light pulses in acute slices (as shown schematically in Figure 3B, left panel). We first
163 performed voltage-clamp whole-cell recordings from Golgi cells surrounded by transfected iNC fibers in
164 GlyT2-cre mice (Figure 3B, right panel). With the use of small collimated beams of light (see *methods*) we
165 stimulated locations near Golgi cell dendrites with a single, short (5 ms) pulses. Inhibitory post-synaptic
166 currents (IPSCs) were evoked in 9 out of 38 recorded Golgi cells (23.7 %; Figure 3C1) with a mean
167 amplitude of 40 ± 28 pA. Given the ionic composition of our experimental solutions, the estimated reversal
168 potential of -74 mV with the permeabilities of bicarbonate and chloride taken into account and the holding
169 potential of -50 mV, the chord synaptic conductance was 1.7 ± 1.2 nS and the slope conductance was 1.9 ±
170 1.3 nS according to the Goldman-Hodgkin-Katz (GHK) equation. We calculated that the equivalent peak
171 conductance of the iNC synapse measured in symmetrical chloride conditions would have been of 8.5 ±
172 5.9 nS. The light-evoked IPSCs had a 10-90% rise time of 2.5 ± 1.3 ms and a bi-exponential decay ($\tau1$ = 8.2
173 ± 1.9 ms, 52.3 ± 18.3 %; $\tau2$= 34.8 ± 9.2 ms, n = 9 cells). Application of strychnine at a concentration
174 selective for glycine receptors (300 nM) decreased the amplitude of the IPSC by 24 ± 25 % ($p = 0.039$, n =
175 9 cells) without affecting the time course of the IPSCs (rise time: 2.4 ± 0.9 ms; decay: $\tau1$ = 9.2 ± 3.0 ms,

176 52.5 ± 23.5 %, τ2 = 40.6 ± 21.2 ms; p = 0.91, p = 0.65 and p = 1.00 respectively, n = 9 cells). These results
177 confirm the presence of a glycinergic component at the iNC-Golgi cell synapses albeit with large variability
178 in its magnitude (range: 0 to 63 %; Figure 3C2, left). Subsequent application of a $GABA_A$-receptor
179 antagonist (gabazine, 2 μM), almost completely blocked the response, decreasing the amplitude of the
180 IPSC by 96.5 ± 2.9 % (p = 0.0078, n = 8 cells; Figures 3C1, C2). These results confirm the mixed GABAergic-
181 glycinergic nature of the iNC axons.

182 To characterize the functional effect of the iNC-originating inhibitory currents on Golgi cells'
183 firing, we recorded Golgi cells in the current-clamp mode in acute slices obtained from GAD-cre mice.
184 Whole-field light stimulation of the iNC axons had a significant effect on the spiking in 24 out of 86
185 recorded Golgi cells (27 %; Figure 3D-G). A single 5 ms light pulse elicited clear inhibitory responses in
186 most of cases, involving a hyperpolarizing postsynaptic potential (n = 12 cells; IPSP amplitude 2.1 ± 1.5
187 mV; Figure 3D) and/or prolongation of the inter-spike interval (ISI) during which the stimulation
188 occurred (n = 15 cells; 60 ± 30 % increase; on average, 223 ± 123 ms ISI increased to 355 ± 286 ms; cells;
189 p = 0.0001, paired t-test; Figures 3E1, 3E2). This inhibition of spiking was more pronounced when iNC
190 fibers were activated with a train of 4-5 light pulses at 50 Hz (pulse duration 10 ms), eliciting a longer
191 spike delay (71 ± 44% increase; n = 16 cells, p < 0.05; Figure 3F). In some of the recorded Golgi cells trains
192 of light pulses elicited a time locking of intrinsic spikes (n = 7, Figure 3 – figure supplement 1) without
193 clear inhibitory effect, suggesting a network effect mediated through the gap junctions among Golgi cells
194 (Dugué et al., 2009; Vervaeke et al., 2010). Taken together, these results demonstrate that the iNC
195 pathway inhibits spiking in Golgi cells.
196

197 **iNC fibers inhibit a subpopulation of Golgi cells with characteristic electrophysiological properties**

198 The rate of success in finding responsive Golgi cells was rather low (24 % and 27 % of all record-
199 ed Golgi cells in GlyT2-cre and GAD-cre mice, respectively) suggesting that iNC axons might preferentially
200 or exclusively inhibit a certain subpopulation of Golgi cells. In the following we will present both electro-
201 physiological and immunochemical evidence supporting this possibility.

202 While analyzing our current-clamp recordings in GAD-cre mice, we noted considerable variability
203 in Golgi cells' properties, with their spontaneous spiking showing the most striking difference (Figure 4A).
204 While 64 out of 85 recorded Golgi cells fired spontaneously at low rates (mean frequency: 9.0 ± 6.5 Hz),
205 the other 21 Golgi cells were quiescent and had a resting membrane potential negative to the spiking

206 threshold (resting potential -55 ± 2.4 mV, spike threshold -43 ± 1 mV, n = 13 cells). When evaluating iNC
207 effects in Golgi cells it became obvious that only the spontaneously active Golgi cells ("s-Golgi cells") were
208 responsive to iNC stimulation. Specifically, 24 out of 64 (37.5 %) s-Golgi cells were inhibited by iNC
209 activation (Figures 4A-B; blue) whereas none of the 21 not-spontaneously spiking Golgi cells ("ns-Golgi
210 cells"; green) were affected by the stimulation. Repeating these stimulations during depolarizing current
211 injections that drove the ns-Golgi cells to continuous spiking also failed to reveal iNC effect (Figure 4A, top
212 right). These findings suggested that iNC fibers inhibit preferentially s-Golgi cells. It should be noted that
213 our virus injections were unlikely to result in transfection of the entire iNC population, hence the
214 observed fraction of inhibited s-Golgi cells is bound to be underestimated.

215 The s-Golgi cells differ from ns-Golgi cells also in action potential (AP) shape (Figure 4D)
216 recorded during steady-state firing. The observation that the AP waveform (composed of AP and AHP)
217 was shorter in s-Golgi cells compared to ns-Golgi cells (Figure 4E; see *Table 3*) led us to seek for other
218 distinguishing electrophysiological features. Compared to the s-Golgi cells, the ns-Golgi cells showed
219 significantly larger variability in all of the AP shape measurements, although no significant differences
220 were found in their average values (see *Table 3*). Also, no differences were found in population averages
221 of the input-output relationship of the two Golgi cell groups, as evidenced by nearly identical current-to-
222 firing frequency (I-F) curves (Figure 4F; *Table 3*). ns- and s-Golgi cells did not differ as a population in
223 their $C_{m,}$ nor in their input resistance, but analysis of their variance showed clear differences between the
224 groups (Figure 4G, compare the significance values obtained with Wilcoxon and F-tests in *Table 3*). The
225 population variability became most visible when comparing the steady-state frequency accommodation
226 (Figure 4H, left, compare the significance values obtained with Wilcoxon and F-tests in *Table 3*): the s-
227 Golgi cells accommodated very uniformly to roughly half of the initial firing frequency, while ns-Golgi cells
228 showed either no adaptation (evidenced by steady-state accommodation values around 90 % of control)
229 or adapted even more than the s-Golgi cells (to 35 % of control; compare the widths of blue and green
230 bars in Figure 4H). The large variability of ns-Golgi cells in frequency accommodation, AHP time, AP half
231 width, C_m, input resistance and AP shape suggest that the ns-Golgi cells form a heterogeneous group of
232 cells consisting of several functionally distinct subpopulations.

233

234 **iNC axons contact Golgi cells with a specific immunohistochemical profile**

235 The results described above suggest that iNC fibers specifically target a subpopulation of

236 spontaneously active Golgi cells with uniform electrophysiological properties. It is well established that
237 Golgi cells are neurochemically heterogeneous (Pietrajtis and Dieudonné, 2012; Ottersen et al., 1988;
238 Simat et al., 2007) . While the majority of Golgi cells express the glycine transporter GlyT2, with most of
239 them being of mixed GABA-glycinergic phenotype, about 15-20 % of Golgi cells are purely GABAergic
240 (Ottersen et al., 1988; Simat et al., 2007) . GlyT2-expressing Golgi cells have previously been reported to
241 be intrinsically silent (Dugué et al., 2009). We thus hypothesized that the iNC-inhibited Golgi cells, all of
242 which fire spontaneously, may correspond to the purely GABAergic Golgi cells. As all of the Golgi cells that
243 express the calcium-binding protein, neurogranin are also GABAergic (Simat et al., 2007), we used
244 neurogranin in conjunction with GlyT2-eGFP expression to differentiate pure GABAergic Golgi cells from
245 the mixed GABA-glycinergic and pure glycinergic Golgi cell populations (Pietrajtis and Dieudonné, 2012;
246 Simat et al., 2007) .

247 We designed a strategy to identify the subtypes of Golgi cells targeted by iNC axons. GlyT2-eGFP
248 transgenic mice (Zeilhofer et al., 2005), in which both mixed GABA-glycinergic and pure glycinergic Golgi
249 cells are labeled with eGFP, were mated with GlyT2-cre animals. The CN of the offspring carrying both
250 transgenes were injected with a floxed AAV expressing the red fluorescent protein tdTomato. Cerebellar
251 cortical sections from these mice were then stained for neurogranin to differentiate between the Golgi
252 cells subtypes. iNC axons were easily identified by their co-expression of eGFP and tdTomato and were
253 found to preferentially contact cell bodies and dendrites of Golgi cells that were intensely stained for
254 neurogranin (Figures 5A-B). This selective targeting of neurogranin-positive cells by iNC fibers extended
255 to the ML (indicated by arrowheads in Figure 5C), as iNC fibers were seen to climb along the apical
256 dendritic shafts of neurogranin-positive Golgi cells to the ML. Similarly, in GAD-cre animals, iNC fibers
257 transfected with YFP and co-stained for GAD65-67 were found to impinge on the dendrites and cell bodies
258 of Golgi cells strongly expressing neurogranin (Figure 5D, arrowheads).

259 In most cases, the innervated Golgi cells were devoid of eGFP staining, suggesting that they are
260 non-glycinergic Golgi cells. However, a few of the iNC-contacted Golgi cells exhibited a low level of eGFP
261 staining in their somata (examples are indicated by asterisks in Figures 5A-B). To distinguish between the
262 eGFP positive and negative Golgi cell subpopulations in a more objective manner, we quantified the
263 normalized mean GlyT2-eGFP and neurogranin staining intensities at the somata of Golgi cells (n = 317
264 cells, n = 13 stacks n = 4 animals; see *methods*). The 2D distribution of the two staining intensities was
265 separated into two populations based on K-means statistical clustering (Figure 5E; Green population: n =

266 238 Golgi cells (75 %); Blue population: n = 79 Golgi cells (25 %); see *methods*). Golgi cells in the two
267 groups differed mainly in their eGFP staining, as illustrated by the bimodal distribution of the mean eGFP
268 intensities (Figure 5F). The normalized neurogranin intensities were approximatetely 50 % higher in the
269 low-eGFP population (Wilcoxon test $p < 0.00001$), even though distributions overlapped extensively
270 (Figure 5G). We thus consider that the blue population of Figure 5 constituting of Golgi cells expressing
271 neurogranin and none or low levels of GlyT2-eGFP, corresponds to the population of Golgi cells releasing
272 principally or exclusively GABA (Aubrey et al., 2007) . For the sake of brevity, we will refer to these cells as
273 "GABAergic Golgi cells" in the following.

274 We counted the iNC appositions found on the somata and large proximal dendrites of each Golgi
275 cell (see *methods*; color-coded in Figure 5H) as a measure of connection strength. Most of the Golgi cells
276 that were contacted by at least one iNC bouton were GABAergic Golgi cells (80 %, n = 32 out of the 40
277 "iNC-contacted" cells; Figure 5H-I). In contrast to the glycinergic Golgi cells that were only rarely apposed
278 to iNC boutons (3 %, n = 8 out of 238 all Golgi cells; on average 1.88 ± 1.12 appositions per cell; max = 4
279 appositions; 15 appositions found overall; Figure 5I, blue dots), 41 % of the GABAergic Golgi cells were
280 contacted by on average 7.65 ± 4.69 appositions (n = 32 out of 79 Golgi cells, max = 20 appositions; 245
281 appositions found overall; Figure 5I, blue dots). These results demonstrate that iNC fibers contact almost
282 exclusively the GABAergic Golgi cell population, as summarized in the schematic drawing of Figure 5J
283 (97% of iNC terminal contact the GABAergic Golgi cell population). To the best of our knowledge, this is
284 the first evidence for differential connectivity among subpopulations of Golgi cells.

285

286 **Bursting activity in iNC neurons and their inhibitory effect on Golgi cell activity *in vivo***

287 The impact of a neuronal pathway depends on properties of transmission at its synapses as well
288 as the firing pattern of its neurons. In the case of the iNC pathway, repetitive stimulation of the axons
289 evoked stronger inhibition of Golgi cells (Figure 3G). To investigate the physiological relevance of such
290 burst activation of iNC axons, we examined the responses of iNC neurons to optogenetic stimulation. First,
291 using acute slices from GlyT2-cre mice transfected as above, we performed extracellular recordings from
292 iNC neurons, identified by their YFP fluorescence. iNC neurons were silent (n = 11 cells) in contrast with
293 the other cell types in the CN (Uusisaari and Knöpfel, 2010, 2012) . Optogenetic excitation of iNC neurons
294 by short light pulses (1 ms) evoked high-frequency bursts of spikes (Figure 6A1). Increasing the
295 illumination power resulted in an increased number of spikes and in mean burst frequency, which

296 saturated around 450 Hz for a light power of 1-2 mW/mm^2 (Figure 6A2; n = 11 cells).

297 To further characterize intrinsic bursting, we performed whole-cell current-clamp recordings
298 from iNC neurons (identified by their fluorescence and lack of spontaneous activity) in slices from
299 transfected GAD-cre mice (Figure 6B1, n = 3 cells). At saturating illumination intensity (1.3 mW/mm^2),
300 stereotypical high-frequency bursts of spikes were evoked with short light durations (10 ms), resembling
301 the extracellular recordings in the GlyT2-cre slices. These bursts were riding on a depolarized plateau
302 which outlasted the illumination period and were often followed by a prolonged depolarized after-
303 potential and low-frequency firing. Increasing the duration of the light pulse extended the burst duration
304 without affecting the intra-burst frequency (Figure 6B2). These results indicate that high-frequency
305 bursting of action potentials could constitute the main firing mode of iNC neurons in response to
306 excitatory synaptic inputs.

307 To investigate the physiological significance of the iNC pathway in an intact cerebellum, we
308 implanted an optical fiber in the CN of virally transfected GlyT2-cre mice to optically activate the iNC
309 neurons, while recording Golgi cell activity (Figure 6C1). Based on our *in vitro* calibration (Figures 6A, B),
310 single 25-ms-long light pulses are expected to evoke short bursts of firing in the iNC neurons. This
311 illumination protocol suppressed spiking in 18 out of 86 recorded Golgi cells (21 %, Figure 6C2, left). The
312 rest of the Golgi cells (79 %, Figure 6C2, middle) as well as PNs (n = 50 cells, Figure 6C2, right) did not
313 show any significant modulation of the spiking frequency following illumination. The time course of the
314 inhibition in the responsive Golgi cells was variable (duration: 23.4 ± 11.7 ms; onset latency: 14.5 ± 7.2
315 ms; peak latency: 25.4 ± 14.1 ms; n = 18, Figure 6D2) as exemplified with colored traces from individual
316 cells in Figure 6D1. The variability of the inhibitory effect can be explained by the variability in iNC spike
317 burst duration that depends on the distance from the optic fiber and thereby stimulation light intensity
318 (Figure 6A). Regardless of this variability, Golgi cells' firing was robustly suppressed (frequency decreased
319 to 1.58 ± 1.46 Hz from a baseline of 10.9 ± 3.9 Hz, n = 18 cells, Figure 6D3). Interestingly, the average
320 firing rate of responsive Golgi cells was significantly higher than the average firing rate of non-responsive
321 Golgi cells (10.5 ± 3.5 Hz, n = 18 cells versus 8.2 ± 4.2 Hz, n = 68 cells, respectively; Wilcoxon test: p =
322 0.036; Figure 6D4). While we cannot make a direct link between the lower firing rate of non-responsive
323 Golgi cells *in vivo* and the quiescence of ns-Golgi cells *in vitro*, these results are supporting the notion that
324 the iNC pathway is targeting a distinct group of Golgi cells.

325 Overall, our results provide the first functional evidence for an inhibitory nucleo-cortical pathway

326 suppressing GABAergic Golgi cell spiking. This pathway likely modulates the inhibitory control of GrCs
327 and thereby gating of sensori-motor inputs into the cerebellar cortex.

328 **DISCUSSION**

329 In the present work, we reveal an inhibitory nucleo-cortical pathway in the cerebellum. This pro-
330 jection is formed by mixed GABA-glycinergic neurons of the CN and targets the GABAergic Golgi cells in
331 the cerebellar cortex.

332

333 **The inhibitory nucleo-cortical (iNC) pathway and identity of the iNC cells**

334 Anatomical demonstrations of nucleo-cortical pathways have appeared in literature already dec-
335 ades ago (Tolbert et al., 1976; Gould and Graybiel, 1976; Dietrichs and Walberg, 1979; Hámori et al.,
336 1980; Buisseret-Delmas, 1988; Batini et al., 1992; reviewed in Haines and Manto, 2009 and Houck and
337 Person, 2013). These classical studies, often ignorant of the afferents' neurotransmitter type, described a
338 range of nucleo-cortical axonal morphologies including rosette-like and simple terminals (Hámori et al.,
339 1980; Tolbert et al., 1980). It was only later established that both glutamatergic (Tolbert et al., 1980;
340 Payne, 1983; Batini et al., 1992; Houck and Person, 2015) and GABAergic (Hámori and Takács, 1988;
341 Batini et al., 1989, 1992; Houck and Person, 2015) CN neurons project to the cortex. Here, using targeted
342 viral transfection and labeling, we demonstrate that the inhibitory nucleo-cortical (iNC) axons originate
343 from a population of mixed GABA-glycinergic CN neurons. The iNC axon terminals were simple in their
344 morphology and rosette-like structures were never observed. Thus, the GABAergic rosette-like terminals
345 found in granule cell layer (GrCL) glomeruli described in earlier works (Chan-Palay et al., 1979; Hámori
346 and Takács, 1988) must arise from extracerebellar sources. The morphology and spread of the iNC axons
347 as well as the axonal bouton size was also different from both the Golgi and Lugaro axons (Dieudonné,
348 1998; Dumoulin et al., 2001).

349 Our study discards the suggestion that inhibitory nucleo-cortical axons would emerge as collat-
350 erals of GABAergic nucleo-olivary (NO) neurons (Figure 1; Tolbert et al., 1978; Haines, 1988). The neurons
351 transfected in the GlyT2-cre animals do not include NO cells, as evidenced by the lack of labeling in the IO
352 (Husson et al., 2014; see also De Zeeuw et al., 1994) and the clear difference in cell body size between
353 GlyT2-cre and NO neurons (Figures 1B-D). While viral transfection protocols used in the GAD-cre mice
354 also transfect NO cells (Lefler et al., 2014; Figure 1A3), all the fibers found in the cortex were GlyT2 im-
355 munopositive, demonstrating that only those GABAergic CN cells that also express GlyT2 project to the

356 cortex. Also, as the purely glycinergic neurons of the medial CN nucleus projecting to the vestibular nuclei
357 (Bagnall et al., 2009) are not found in the main targets of viral transfections in the present study (inter-
358 positus and lateral CN), they are unlikely to be the source of the iNC axons.

359 The nucleo-cortical axons in both GlyT2-cre and GAD-cre models were very similar in shape and
360 function and co-stained for GAD and GlyT2, respectively (Figure 2). The small differences observed are
361 likely to originate from variability in fixation procedures and wavelength dependence of optical resolu-
362 tion. Therefore, iNC fibers undoubtedly represent the axons of a single mixed CN neuron type. The density
363 of nucleo-cortical fibers in the GAD-cre model was somewhat higher than in the GlyT2-cre model (com-
364 pare panels 2A1 and 2B1), most likely due to the mosaic expression of cre in only 50% of mixed neurons
365 in the GlyT2-cre mice (Husson et al., 2014) as well as the stronger expression levels obtained with the
366 AAV9 serotype virus used in the GAD-cre model.

367 The iNC neurons described in the present work show clear morphological (Figure 1B2) and elec-
368 trophysiological (Figure 6) resemblances to the CN glycinergic neurons described in two recent studies as
369 spontaneously inactive, mixed GABA-glycinergic neurons (compare the present results with Figure 1 in
370 Uusisaari and Knöpfel, 2010 and Figure 7Ab in Husson et al., 2014). Thus, we conclude that the iNC neu-
371 rons, the "Gly-I" neurons and the mixed GABA-glycinergic neurons are the same cells. While these neurons
372 also have local axon collaterals within in the CN (Husson et al., 2014), their projection to the cortex is their
373 most distinguishing feature. Thus we propose that they should be referred to as "inhibitory nucleo-
374 cortical" (iNC) neurons.

375

376 **Diversity of Golgi cells and their inhibitory control**

377 Golgi cells have previously been shown to receive inhibitory synapses from both Lugaro and oth-
378 er Golgi cells in the cerebellar cortex. We demonstrate here that single iNC projection axons form numer-
379 ous terminal swellings on the somata and dendrites of Golgi cells (Figure 2), somewhat reminiscent of the
380 climbing fiber articulation on Purkinje cells. Specific optogenetic stimulation of the iNC axons evoke IPSCs
381 mediated both by $GABA_A$ and glycine receptors (Figure 3), in line with the immunohistochemical evidence
382 that iNC terminals contain both GABA and glycine (Figures 2D-E). The average synaptic conductance at
383 the iNC synapses (estimated to be 1.9 and 8.5 nS in physiological and symmetrical chloride, respectively)
384 is about six times the conductance reported at unitary Golgi-Golgi synapses (0.33 nS in physiological chlo-
385 ride; Hull and Regehr, 2011) and similar to the conductance at Lugaro to Golgi cell synapses in the juvenile

386 animal (Dumoulin et al., 2001). As our spatially restricted light stimulation likely activated a single or only
387 a few iNC axons, the evoked IPSCs likely represent unitary responses through the multiple contacts made
388 by single axons on Golgi cells.

389 Most of the current physiological work on Golgi cells tends to assume a homogeneous neuronal
390 population while simultaneously using various, partly contradictory, identification criteria to target them
391 for experiments (Schulman and Bloom, 1981; Holtzman et al., 2006; Xu and Edgley, 2008; Hull and
392 Regehr, 2011; Hull et al., 2013). However, accumulating evidence indicates that Golgi cells can be divided
393 into different groups based on their neurotransmitter content (GABA, glycine or both; Ottersen et al.,
394 1988) as well as specific molecular marker expression (Simat et al., 2007; Dugué et al., 2009; Pietrajtis
395 and Dieudonné, 2013). By demonstrating that the Golgi cells contacted by the iNC axons are characterized
396 by none or low level of GlyT2-eGFP staining as well as high neurogranin expression (Figure 5; compare
397 with "type 4" Golgi cells in Simat et al., 2007), we present the first evidence that neurochemical subtypes
398 of Golgi cells may participate in specific microcircuits.

399 Our work further supports the functional specialization of purely GABAergic Golgi cells by show-
400 ing that they can be distinguished from other Golgi cells based on their electrophysiological properties
401 (Figure 4). A previous work showed that glycinergic (GlyT2-eGFP positive) Golgi cells are not spontane-
402 ously active *in vitro* (Dugué et al., 2009). Here we show that spontaneously spiking Golgi cells (s-Golgi
403 cells), unlike the not-spontaneously spiking Golgi cells (ns-Golgi cells), receive functional synaptic con-
404 tacts from the iNC fibers (Figure 3). s-Golgi cells had relatively uniform properties (Figure 4), confirming
405 their identification as a distinctive functional group. In contrast, ns-Golgi cells varied in all of the examined
406 features (Figure 4 and Table 3) suggesting that this population may be further divided into several func-
407 tional subgroups. The functional microcircuit of the GrCL thus needs to be re-examined in the light of the
408 existence of multiple Golgi cell subtypes.

409

410 **Physiological significance of the iNC pathway**

411 Optogenetic activation of iNC axons was found to modulate Golgi cell discharge *in vitro* and *in vivo*
412 (Figures 3 and 6). The most common effect was a short-latency inhibition of spiking (Figures 3E-H). *In*
413 *vivo* inhibition of spiking could last for tens of milliseconds, most likely due to the iNC neurons' propensity
414 for high-frequency burst firing (Figure 6) and to the slow kinetics of the relatively large synaptic conduct-
415 ances at iNC to Golgi cell synapses (Figure 3).

416 Although the iNC axons may represent less than 5 % of the afferent fibers in the GrCL (Hámori et
417 al., 1980; Legendre and Courville, 1986), the ramification of iNC axons, the high divergence of the Golgi
418 cell axon and the electrical coupling between Golgi cells (Dugué et al., 2009) will amplify the potency of
419 the iNC effects on the GrCL network. The anatomical and electrophysiological evidence presented here
420 suggests that the iNC pathway is likely to induce a period of disinhibition in the GrCs. This disinhibition
421 could influence the time-window for MF input integration in GrCs, enhancing GrC excitability and thereby
422 facilitate the activation of PNs (Chadderton et al., 2004; Kanichay and Silver, 2008; D'Angelo and De
423 Zeeuw, 2009). Confirmation of this functional significance will require experimentation in awake animals,
424 as the MF/PF pathway is known to be quiescent in anaesthetized animals (Bengtsson and Jörntell, 2007;
425 Wilms and Häusser, 2015) and no modulation of PN spiking is thus expected by the disinhibition of GrCs
426 (Figure 6C2).

427 No iNC axons were found outside the cerebellar structures in the GlyT2-cre model, and no evi-
428 dencee for iNC contacts on cerebellar granule cells was seen, excluding the possibility of extracerebellar or
429 parallel fiber effects on Golgi spiking. However, the glutamatergic projection neurons of the CN collateral-
430 ising as an excitatory nucleo-cortical ("eNC") pathway that contact the neurogranin-positive Golgi cells
431 (Tolbert et al., 1976, 1977, 1978; Hámori et al., 1980; Payne, 1983; Houck and Person, 2013, 2015) may be
432 contacted by local iNC axons. The iNC synapses on the eNC neurons constitute only of a tiny fraction of
433 their synaptic inhibition (Husson et al., 2014), but we cannot completely exclude that some facet of the
434 iNC-mediated depression of Golgi cell spiking *in vivo* may reflect a decrease in excitatory synaptic drive
435 from CN-originating mossy fibers. However, it is unlikely that the short bursts of iNC spikes evoked by our
436 stimulation protocol would result in a long pause in spiking of CN projection neurons as they are extreme-
437 ly resistant to inhibition (Person and Raman, 2012; Chaumont et al., 2013; Najac and Raman, 2015). A
438 short delay in eNC spikes is unlikely to be the principal source of the observed Golgi cell inhibition, unless
439 the Golgi cell activity would be to a large extent determined by CN. Thus, while further work elucidating
440 the functional role of the eNC projection to the cerebellar granule cell layer is sorely needed, we conclude
441 here that the inhibition of Golgi cell spiking observed *in vivo* (Figure 6) is mainly caused by a direct inhibi-
442 tion by the iNC axon terminals impinging on Golgi cell dendrites and cell bodies.

443 A major feature of the iNC projection to the cortex is its divergence: upon relatively localized viral
444 injection in the CN entire lobules may be innervated. Furthermore, single iNC axons traverse long distanc-

445 es along the medio-lateral plane, similarly to the parallel fibers (PF), making numerous contacts on indi-
446 vidual Golgi cell dendrites. Such an arrangement could partly explain the synchronization of Golgi cell
447 activity observed along the axis of the lobules (Vos et al., 1999). Furthermore, disinhibition of GrCs by iNC
448 axons could enhance and synchronize MF-PF transmission specifically along medio-lateral stripes, possi-
449 bly contributing to on-beam synchronization of PNs (Heck and Thach, 2007). iNC neurons may thus im-
450 plement refined temporal binding of parasagittal cerebellar modules within a lobule. Intriguingly, while
451 the iNC neurons, like all other CN neurons examined so far, are contacted by PN axons (Figure 1 – figure
452 supplement 1; compare with Bagnall et al., 2009), their intrinsic quiescence (Uusisaari and Knöpfel, 2010;
453 Figure 6) calls for identification of the sources of synaptic excitation, as they will determine the context
454 within which Golgi cells would be inhibited. Possible candidates include the collaterals of CFs, MFs and the
455 local axons of CN neurons. While there is no direct evidence either for or against any of these sources, a
456 few earlier works have described inhibition of Golgi cells in response to electrical stimulation of the IO or
457 to sensory stimulation (Schulman and Bloom, 1981; Xu and Edgley, 2008), suggesting that the IO might be
458 the source of excitatory drive for iNC neurons.

459 Cerebellar granule cell layer gating by Golgi cell network has been postulated for a long time to
460 play a critical role in cerebellar function; however, the absence of experimental tools allowing specific
461 control of the Golgi network during behavior has prevented investigation of this hypothesis. The novel,
462 inhibitory pathway from the CN to the Golgi cells revealed in our present work opens a way for targeted
463 manipulation and analysis of the information gating in the cerebellar granule layer. Furthermore, it is now
464 reasonable to assert that through iNC neurons as well as the collateralization of glutamatergic projection
465 neurons to the GrCL (Houck and Person, 2015), the CN hold a key position to control the activity of the
466 cerebellar cortex.
467

468
469 **MATERIALS AND METHODS**

470

471 **Animals:** All experiments were performed on adult mice (P > 30 days; both males and females) of two
472 mouse lines: the GAD-ires-cre (Taniguchi et al., 2011) and the GlyT2-cre (Husson et al., 2014). These cre-
473 lines, combined with floxed adeno-associated viral (AAVs; see Table 1 for details) injections into the CN,
474 allowed specific transfection of either GABAergic or glycinergic CN neurons, respectively. In addition, for
475 immunostaining experiments, heterozygous GlyT2-cre mice were bred with GlyT2-eGFP transgenic mice
476 (Zeilhofer et al., 2005) and the offspring carrying both GlyT2-cre and GlyT2-GFP genes were transfected as
477 above. Retrograde labeling of the nucleo-olivary neurons (Figures 1C-D) was performed in adult wild-type
478 C57BL/6 mice via non-floxed viral injection into the inferior olive. For Figure 1 – figure supplement 1,
479 adult L7-CHR2-YFP mice (Chaumont et al., 2013) were bred with GlyT2-eGFP mouse and double-positive
480 offspring were used for optogenetic experiments. All animal manipulations were made in accordance with
481 guidelines of the Centre National de la Recherche Scientifique and the Hebrew University's Animal Care
482 and Use Committee.

483

484 **Stereotaxic injections:** Mice were deeply anesthetized with a mixture of ketamine and xylazine (106
485 mg/kg and 7.5 mg/kg, respectively) and placed in a stereotaxic frame. Small craniotomies were per-
486 formed above the cerebellar nuclei (CN). The target regions were mostly in the lateral and interpositus
487 nuclei, and the injections were performed unilaterally for immunohistochemical and anatomical proto-
488 cols, and bilaterally for electrophysiological experiments. A quartz capillary pipette (35-40 μm tip diame-
489 ter) was positioned in the brain at the proper coordinates for CN (1.8 - 2.2 mm lateral from midline, 3.2 -
490 3.4 mm deep, 6.0 - 6.2 mm from Bregma) and small amount (50 to 300 nl for electrophysiological experi-
491 ments, 50-100 nl for immunohistochemical protocols) of viral suspension (summarized in Table 1) was
492 slowly pressure-injected either by a hand-held syringe or using a Picospritzer II (General Valve Corpora-
493 tion). In some experiments, additional virus (either non-specific or cre-dependent GFP reporter) was in-
494 jected in several locations in the cerebellar cortex or into the inferior olive. When the entire volume was
495 injected, pipettes were held at the same position for 10 to 15 minutes and were then carefully and slowly
496 removed from the tissue, in order to avoid backflow of the viral suspension and unwanted contamination
497 in the cerebellar cortex along the pipette tracts. Animals were closely monitored for three days until re-

498 covery from surgery and then housed for at least three to four weeks before being used in experiments, as
499 described below. Throughout this report, we refer to data obtained using the GAD-cre mouse cerebella
500 injected with floxed AAV2/9 virus with mCherry and ChR2 in the CN as "GAD-cre", and that from GlyT2-
501 cre mouse cerebella injected with floxed AAV2/1 virus with EYFP and ChR2 as "GlyT2-cre", unless other-
502 wise specified.
503
504 **Acute slice preparation:** 300 μm thick cerebellar slices were cut from the GAD-cre or GlyT2-cre cerebella
505 using the Campden 7000smz oscillating blade microtome and ceramic blades (Campden Instruments, UK).
506 For the experiments performed at HUJI (GAD-cre animals), horizontal slices were prepared at physiologi-
507 cal temperature as described previously (Huang and Uusisaari, 2013; Ankri et al., 2014) and incubated in
508 Solution 1. For the experiments performed at IBENS (GlyT2-cre animals), sagittal slices were prepared
509 using ice-cold Solution 2. After cutting, the slices were rinsed in warm Solution 3 for few seconds before
510 being transferred to a recovery chamber with Solution 4. Table 2 summarizes the ionic compositions of all
511 experimental solutions. Acute slices of L7-ChR2-YFP x GlyT2-eGFP animals used for Figure 1 – supplement
512 figure 1 were prepared similarly. Notably, in all experiments, the extent of viral transfection was carefully
513 examined in all slices to make sure no unwanted cerebellar structures were labeled.
514
515 ***In vitro* electrophysiological recordings:** The slices were incubated for at least 30 minutes to an hour in
516 physiological temperature (Huang and Uusisaari, 2013; Ankri et al., 2014) before being transferred to a
517 recording chamber, mounted on an Olympus (BX51WI or BX61WI) microscope equipped with an epifluo-
518 rescence illumination pathway (Roper Scientific, Photometrics, Tucson, AZ) and a camera (Vx45; Optronix,
519 Goleta, CA). During experiments, the GAD-cre slices were perfused with room-temperature Solution 1 (25-
520 28°C; flow rate 3 ml/min) and the GlyT2-cre slices were perfused with Solution 4 at physiological temper-
521 ature (33°C; flow rate 3.5 ml/min). The bicarbonate-buffered solutions (1 and 4) were continuously
522 gassed with 5% O_2/95% CO_2. Borosilicate glass patch electrodes (resistance 3-12 MΩ) were filled with
523 intracellular solution (see *Table 2*; pH 7.3, 280 mOsm). For selecting region for patch-clamp experiments,
524 as well as ascertaining that there was no transfection of any cortical neurons, slices were visualized with
525 arc-lamp illumination and appropriate filters (for mCherry fluorescence in GAD-cre brains, emission: 605–
526 685 nm, excitation: 530–588; GFP fluorescence: excitation: 473-508 nm; emission: 518-566 nm, for YFP
527 fluorescence in GlyT2-Cre brains, emission: 523- 563 nm; excitation: 500-523 nm). Whole-cell patch-

528 clamp recordings, both current clamp and voltage clamp, were acquired using a Multiclamp 700B amplifi-
529 er (Molecular Devices, Sunnyvale, CA), digitized at 10 kHz (current clamp experiments) or 50 kHz (voltage
530 clamp experiments) with USB-6229 acquisition board (National Instruments, Austin, Texas) and low-pass
531 filtered at 2 kHz. Golgi cells were unambiguously identified from other cells in the cerebellar granular cell
532 layer by the size of their soma and their bi-exponential capacitive current (Dieudonné, 1995); further-
533 more, in some experiments using the GAD-cre mice, additional cre-dependent reporter virus was used to
534 label GABAergic Golgi cells in the cortex and was used to guide neuronal selection. Thus, the percentage of
535 s-Golgi cells out of all Golgi cells recorded (Figure 4) was biased towards GABAergic Golgi cells.
536 In the current-clamp experiments, intrinsic electrophysiological properties and synaptic inputs were as-
537 sessed in Golgi cells either with zero holding current or with negative current injection so that the sponta-
538 neously spiking Golgi cells were hyperpolarized to subthreshold voltage values (-55 mV to -60 mV), simi-
539 lar to the resting membrane potential of the not-spontaneous Golgi cells. During voltage-clamp experi-
540 ments, Golgi cells holding potential was -50 mV. All experiments were performed in the presence of 20 μM
541 D-2-amino-5-phosphonopentoate (D-APV, Abcam or Sigma Aldrich) and 10 μM 6-cyano-7-
542 nitroquinoxaline-2,3-dione (CNQX, Sigma Aldrich) or 10 μM 2,3-dihydroxy-6-nitro-7-sulfamoyl-
543 benzo[f]quinoxaline-2,3-dione (NBQX, Abcam) to block N-Methyl-D-aspartic acid (NMDA) and α-Amino-3-
544 hydroxy-5-methyl-4-isoxazolepropionic acid (AMPA) receptors, respectively. In some experiments,
545 strychnine (Abcam or Sigma Aldrich) and SR 95531 ("gabazine"; Abcam or Sigma Aldrich) were added to
546 the bath. Regarding Figure 1 – figure supplement 1, slice perfusion system was similar to what described
547 above. GlyT2-eGFP positives neurons were identified in the CN by epifluorescence and recorded (holding
548 potential - 60 mV, intracellular solution as described in Husson et al., 2014) .
549
550 ***In vitro* optogenetic stimulation:** For optogenetic activation of channelrhodopsins (ChR2) in acute GAD-
551 cre slices, whole-field band-pass-filtered Hg-lamp (Oregon Green filter 473-508 nm; ~5 mW/mm^2) was
552 used, while for the GlyT2-cre slices an optical system combining low-numerical aperture (NA) Gaussian
553 beam illumination and fast acousto–optic focusing system with a 473 nm continuous-wave diode-pumped
554 solid-state laser (LRS 0473-00100-03, Laserglow Technologies) was used as a one-photon light source.
555 Small field of view (1.35 μm x 1.08 μm) around the ChR2-expressing fibers was stimulated (stimulation
556 duration 5 ms; inter-stimulation interval 20 s). PN terminals in the cerebellar nuclei of L7-ChR2-YFP x

557 GlyT2-eGFP mouse (Figure 1 – figure supplement 1) were stimulated with 470 nm LED whole-field illumi-
558 nation (Thorlabs) with one millisecond duration.
559 Throughout the work, special care was taken to prevent inadvertent transfection and stimulation of other
560 inhibitory cerebellar interneurons expressing GAD and GlyT2 in our two mouse models. In addition to the
561 precautions taken during the stereotaxic injection procedures, during acute experiments, the slices were
562 carefully and systematically examined before being used for electrophysiological experiments; if unin-
563 tended labeling was present, the slices were discarded. Finally, before patch-clamping a Golgi cell, the
564 morphology and location of the fibers was carefully examined in order to exclude the possibility of activat-
565 ing parasagittal long-range Lugaro axons.
566
567 ***In vitro* data analysis**: Electrophysiological data were analyzed with Igor Pro 6.1 (Wavemetrics, Portland,
568 OR) and MATLAB R2009b (MathWorks, Natick, MA). Statistical analysis was performed using R GNU and
569 Matlab R2009b or R2012b. Data are presented in the text as mean ± S.D, unless otherwise specified. For
570 statistical significance, Wilcoxon rank-sum, two-tailed student's t-test (paired or unpaired), F-test, K-S test
571 and signed-rank tests were used, as applicable, taking into account possible assumptions of normality as
572 mentioned in the results. Spike delay analysis was performed by aligning the last spikes before light stim-
573 ulation in each trace for each cell and measuring the time to the next spike after light stimulation; the
574 measurements were normalized to the cell's average inter-spike interval. For comparing electrophysiolog-
575 ical properties of different types of Golgi cells, grand average action potential (AP) waveforms were gen-
576 erated for each cell by averaging peak-aligned APs obtained during 1-s voltage sweeps while adjusting the
577 firing frequency to ~25 Hz with current injection as necessary, and then by averaging these peak-aligned
578 mean waveforms across experiments. Estimated capacitance (C_m) was defined as the ratio of membrane
579 resistance (R_m) and time constant (τ), estimated from voltage responses (< 5 mV) to small hyperpolarizing
580 current steps that did not activate voltage-gated conductances (evidenced by the good single-exponential
581 fits to the voltage responses). AP threshold was defined as the voltage at the time of the main peak in the
582 second derivative of the voltage trace; AP amplitude was measured as the voltage difference between the
583 spike threshold and peak voltage. Spike half-width was measured spike duration at half-amplitude. Spike
584 after-hyperpolarization (AHP) voltage was measured at the post-spike minimum voltage. AHP time was
585 measured as the time of AHP voltage after threshold, and AHP amplitude was measured as the difference
586 of the AHP voltage and spike threshold voltage. For fair comparison of current-to-firing frequency ratios

587 in different sized cells, the current injection values were normalized to the C_m of each cell. Spike frequency
588 adaptation index was quantified as the relative decrease in instantaneous firing frequency during a 1-s
589 long depolarizing current step (from -65 mV holding level) during which the mean firing frequency was
590 ~25 Hz. In the pharmacological voltage-clamp experiments (Figure 3), the responses were recorded after
591 at least 6 minutes from the beginning of the perfusion of the drug into the recording chamber to provide
592 the time for the steady state effect. Time-locking of spikes (Figure 3 - figure supplement 1) was quantified
593 as the decrease in the normalized Vm variability between subsequent stimulation trials. Decrease in vari-
594 ability, as an index of spike-time locking, was considered statistically significant at the level of 3 SD (see
595 also Schneider et al., 2014).
596
597 ***In vivo* electrophysiological recordings and data analysis:** Animals were placed in a stereotaxic appa-
598 ratus (Harvard Apparatus). A scalp incision was made along the midline; the skull was cleaned by scraping
599 and by application of hydrogen peroxide. Crus I and II were exposed with a craniotomy but the dura was
600 not removed to enhance mechanical stability. Commercial tetrodes embedded in a quartz tube (Thomas
601 Recording, Giessen, Germany), gold-plated to reach a 100–200 kΩ impedance, were lowered into the CN.
602 Signals were referenced against a tungsten electrode positioned in saline at the surface of the cerebellar
603 cortex. The light was delivered immediately above the CN via an optical fiber (diameter 200-μm core)
604 connected to CrystaLaser at 473 nm and inserted in a cannula placed above the injection sites in the CN
605 (see "Stereotaxic injections" paragraph for coordinates). 25-50ms light pulses (45 mW) were delivered at
606 4 Hz in 3 s bouts separated by 7 s recovery periods; post-hoc inspection showed no indication of de-
607 creased inhibition during the 3 s bouts, suggesting that these stimulation parameters did not induce cu-
608 mulative ChR2 inactivation. Signals were acquired using a custom-made headstage and amplifier and a
609 custom-written Labview software (National Instruments, Austin, TX) allowing real time monitoring of
610 cellular activity. To isolate spikes, continuous wide-band extracellular recordings were filtered off-line
611 with a Butterworth 1 kHz high pass filter. Spikes were then extracted by thresholding the filtered trace
612 and the main parameters of their waveform extracted (width and amplitude on the 4 channels). The data
613 were hand-clustered by polygon-cutting in 2-dimensional projections of the parameter space using Xclust
614 (Matt Wilson, MIT). The quality of clustering was evaluated by inspecting the auto-correlograms of the
615 units (Gao et al., 2011). Golgi cells and Purkinje cells were isolated according to most recently published
616 criteria (Van Dijck et al., 2013). These criteria provide a simple approach to classify cerebellar units using

617 only a few statistical parameters describing the firing frequency and irregularity of discharge: the mean
618 spike frequency (MSF), the coefficient of variation of the log of the interspike interval (LCV) and entropy
619 of the interspike intervals (ENT). We used the boundaries values on these parameters defined by Van
620 Dijck et al., 2013 to identify Golgi cells (MSF < 20 Hz, 0.5 < ENT < 7.5 and 0.02 < LCV < 0.25). Golgi cells
621 exhibited an average firing rate of 8.7 ± 4.2 Hz. To assess the presence of a response to optogenetic stimu-
622 lations, peri-stimulus time histograms (PSTH) were constructed. Each PSTH was normalized by subtract-
623 ing the average baseline spike count (before stimulation) and dividing by the baseline standard deviation
624 yielding a z-score. A modulation of firing rate in response to optogenetic stimulation was considered sig-
625 nificant when the absolute Z-score of a 3 ms bin was higher than 2.5 in at least two time bins in the 50 ms
626 time window following the stimulus. The total time during which the Z-score was significant defined the
627 duration of the inhibition. The latencies (onset and peak) were calculated starting from the beginning of
628 the light-pulse, the peak latency being the point where the Z-score was maximal and the onset latency
629 being defined as the first time point with a significant z-score.
630
631 **Anatomical examination and immunohistochemistry:** Animals were deeply anesthetized with intra-
632 peritoneal injection of sodium pentobarbital (50 mg/kg) and perfused through the aorta with ice-cold
633 solution of phosphate buffer saline (PBS; pH 7.4; Sigma) followed by 50-75 ml of 4% w/v paraformalde-
634 hyde (PFA; VWR) in PBS. The entire brain was then dissected and post-fixated (3h for immunohistochem-
635 istry, overnight for anatomical examination) in 4 % PFA at 4°C before rinsing in PBS. For anatomical con-
636 focal imaging, 80 µm sections were cut with a Leica 1000TS vibratome (Leica Microsystems), placed on
637 objective glass, mounted with Immu-Mount (Thermo Scientific) and coverslipped with #1.5 glass. For
638 immunohistochemistry experiments, the brains were cryoprotected by equilibration in 30 % sucrose w/v
639 PBS at 4°C and then cut at -20 °C with a Leica CM3050S cryostat (Leica Microsystems, Wetzlar, Germany).
640 Free-floating 80 µm thick parasagittal sections were rinsed in PBS and permeabilized 2 hours at room
641 temperature in 0.4 % v/v Triton 100-X (Sigma) in PBS. Non-specific sites were saturated by incubation in
642 0.4 % Triton 100-X - 1.5 % cold fish skin gelatin (Sigma) in PBS at room temperature for 3 hours. Primary
643 antibodies were applied overnight at 4°C in a PBS solution containing 0.1 % Triton 100-X - 1.5 % fish gela-
644 tin (mouse GAD65-67 antibody mAB 9A6 (Enzo Life Sciences, Farmingdale, NY) at 1/500 final dilution;
645 chicken GFP antibody (Avès, Oregon, USA) at 1/1000 final dilution; guinea pig VIAAT antibody (Synaptic
646 Systems) at 1/1500 final dilution; guinea pig GlyT2 antibody (Millipore) at 1/1500 final dilution, rabbit

647 Neurogranin antibody (Millipore, Darmstadt, Germany) at 1/500 final dilution). After rinsing in 0.1 %
648 Triton 100-X in PBS, slices were incubated overnight at 4°C with secondary antibodies coupled to 488,
649 549 or 649 DyLight fluorophores (Jackson ImmunoResearch, West Grove, PA) or Alexa Fluor 555 IgG
650 (Invitrogen, Carlsbad, CA) at 1/500 final dilution in PBS - 0.1% Triton 100-X -1.5 % cold fish skin gelatin.
651 Slices were finally rinsed with PBS and mounted in Prolong Gold Antifade Reagent (Sigma). For Figure 1 –
652 figure supplement 1, immunostaining against GFP and VIAAT (same antibodies as above) were performed
653 on paraffin-embedded sections as previously described (Husson et al., 2014).
654
655 **Image acquisition and Analysis:** Confocal stacks from immunolabeled cerebellar slices were acquired
656 using an inverted confocal microscope (Leica, SP8) using a 63X oil immersion objective (NA 1.3). Confocal
657 stacks for anatomical visualizations were acquired with Leica SP5 microscope using 40x (NA 1.25) and
658 63x (NA 1.5) oil-immersion objectives, with 8 or 12 bit color depth, and with 0.1 µm z-step. The images
659 were acquired for mCherry, EYFP and GFP fluorescence with excitation lasers and emission filters set to:
660 561 DPSS laser, 587–655 nm; 488 Argon laser, 520-580 nm; GFP, 500-550 nm. Wide-view images (in Fig-
661 ure 2A1 and B1) were composed by merging tiles of confocal stacks (with 10 % overlap and 1 um z-step).
662 The grayscale background images in 2A1 and B1 were obtained from autofluorescence signals acquired at
663 the same time as the specific fluorescence signals. Morphological features (NC cell body sizes, iNC axonal
664 bouton sizes) were measured using the Fiji image analysis software (Schindelin et al., 2012). The soma
665 sizes are given as the major length axis; for axon bouton sizes, as the area of the cross section of each bou-
666 ton in maximal projection image. To quantify neurogranin and GlyT2-eGFP staining intensities at Golgi cell
667 bodies, z-stacks containing the somata were projected and averaged (z-projection thickness: 6.8 µm).
668 Intensities for each channel were normalized according to the slope of the fit to the logarithmic distribu-
669 tion of their pixel intensity before being retrieved and the ratios were calculated. As the neuropil in cere-
670 bellar granule layer is densely labeled in the GlyT2-eGFP mice preventing backtracking individual distal
671 dendrites to their somata in order to attribute them a ratio value, the iNC varicosities in the granular cell
672 layer were included in the statistics only when contacting proximal dendrites and cell bodies. Using GNU
673 R, K-means 2D clustering was performed on mean GlyT2-eGFP versus mean neurogranin dataset to clus-
674 ter the GoC subpopulation.
675

ACKNOWLEDGEMENTS

We thank all members of the Yarom laboratory, and especially Avi Libster and Vitaly Lerner, for helpful discussions and support with technical issues; and Dr. Naomi Melamed-Book (ELSC Bio-Imaging unit) for assistance with confocal imaging. We thank Dr. Karl Deisseroth and Dr. Edward Boyden for MTAs of adeno-associated-viruses. Research was supported by CNRS, INSERM and ENS, and by Agence Nationale de la Recherche Grants INNET (BL2011) and Edmond and Lily Safra Center for Brain Sciences (ELSC). We are grateful to the IBENS Imaging Facility, which received the support of grants from the "Région Ile-de-France" (NERF N°2009-44 and NERF N°2011-45), the "Fondation pour la Recherche Médicale" (N° DGE 20111123023) and the "Fédération pour la Recherche sur le Cerveau - Rotary International France" (2011). The IBENS Imaging Facility has also received support implemented by the ANR under the program «Investissements d'Avenir», with the references: ANR-10-LABX-54 MEMO LIFE, ANR-11-IDEX-0001-02 PSL* Research University and ANR-10-INSB-04-01 France-BioImaging infrastructure. ZH was a recipient of a fellowship from Université Pierre et Marie Curie – ED3C. KP was supported by FRM and Labex MemoLife. LA was supported by Rafik, the Edmond and Lily Safra Center for Brain Sciences (ELSC) and the Benin foundation. MYU was supported by ELSC and CEREBNET (PITN-GA-2009-238686). The work by LA, YY and MYU was also supported by the Gatsby Charitable Foundation.

COMPETING INTERESTS

The authors declare no competing financial or intellectual interests.

1. **Andersen BB, Korbo L, Pakkenberg B**. A quantitative study of the human cerebellum with unbiased stereological techniques. *J. Comp. Neurol.* 326: 549–60, 1992. doi: 10.1002/cne.903260405.
2. **Angaut P, Cicirata F, Serapide F**. Topographic organization of the cerebellothalamic projections in the rat. An autoradiographic study. *Neurosci.* 15:389-401, 1985. doi:10.1016/0306-4522(85)90221-0.
3. **Ankri L, Yarom Y, Uusisaari M**. Slice It Hot: Acute Adult Brain Slicing in Physiological Temperature. *JoVE* 92, 2014. **doi:** 10.3791/520688.
4. **Aoki S, Sato Y, Yanagihara D**. Effect of inactivation of the intermediate cerebellum on overground locomotion in the rat: A comparative study of the anterior and posterior lobes. *Neurosci. lett.* 576: 22-27, 2014. doi:10.1016/j.neulet.2014.05.027.
5. **Apps R, Garwicz M**. Anatomical and physiological foundations of cerebellar information processing. *Nat. Rev. Neurosci.* 6: 297–311, 2005. doi: 10.1038/nrn1646.
6. **Apps R, Hawkes R**. Cerebellar cortical organization: a one-map hypothesis. *Nat. Rev. Neurosci.* 10: 670–681, 2009. doi: 10.1038/nrn2698.
7. **Asanuma C, Thach WT, Jones EG**. Nucleus interpositus projection to spinal interneurons in monkeys. *Brain research* 191: 245-248, 1980. doi:10.1016/0006-8993(80)90327-3.
8. **Aubrey K, Rossi F, Ruivo R, Alboni S, Bellenchi G, Goff A, Gasnier B, Supplisson S**. The Transporters GlyT2 and VIAAT Cooperate to Determine the Vesicular Glycinergic Phenotype. *J Neurosci.* 27: 6273–6281, 2007. doi: 10.1523/JNEUROSCI.1024-07.2007.
9. **Bagnall MW, Zingg B, Sakatos A, Moghadam SH, Zeilhofer HU, du Lac S**. Glycinergic projection neurons of the cerebellum. *J. Neurosci.* 29: 10104-10110, 2009. doi: 10.1523/JNEUROSCI.2087-09.2009.
10. **Batini C, Buisseret-Delmas C, Compoint C, Daniel H**. The GABAergic neurones of the cerebellar nuclei in the rat: projections to the cerebellar cortex. *Neurosci. lett,* 99: 251-256, 1989. doi: 10.1016/0304-3940(89)90455-2.
11. **Batini C, Compoint C, Buisseret-Delmas C, Daniel H, Guegan M**. Cerebellar nuclei and the nucleocortical projections in the rat: Retrograde tracing coupled to GABA and glutamate immunohistochemistry. *J. Comp. Neurol.* 315: 74–84, 1992. doi: 10.1002/cne.903150106.
12. **Bazzigaluppi P, Ruigrok T, Saisan P, De Zeeuw C, Jeu M**. Properties of the Nucleo-Olivary Pathway: An In Vivo Whole-Cell Patch Clamp Study. *PLoS ONE* 7, 2012. doi: 10.1371/journal.pone.0046360.
13. **Bengtsson F, Hesslow G**. Cerebellar control of the inferior olive. *The Cerebellum,* 5:7-14, 2006.
14. **Bengtsson F, Jörntell H**. Ketamine and xylazine depress sensory-evoked parallel fiber and climbing fiber responses. *J neurophys*, 98(3): 1697-1705, 2007. doi: 10.1152/jn.00057.2007.
15. **Buisseret-Delmas C**. Sagittal organization of the olivocerebellonuclear pathway in the rat. I. Connections with the nucleus fastigii and the nucleus vestibularis lateralis. *Neuroscience research*, 5: 475-493, 1988. doi: 10.1016/0168-0102(88)90038-7.
16. **Chadderton P, Margrie TW, Häusser M**. Integration of quanta in cerebellar granule cells during sensory processing. *Nature*, 428: 856-860, 2004. doi: 10.1038/nature02442.
17. **Chan-Palay V**. The cerebellar dentate nucleus, *Springer-Verlag*, Berlin, 1977. doi: 10.1007/978-3-642-66498-4_1.
18. **Chan-Palay V, Palay S, Wu J**. Gamma-aminobutyric acid pathways in the cerebellum studied by retrograde and anterograde transport of glutamic acid decarboxylase antibody after in vivo injections. *Anat Embryol* 157: 114, 1979.
19. **Chaumont J, Guyon N, Valera A, Dugué G, Popa D, Marcaggi P, Gautheron V, Reibel-Foisset S, Dieudonné S, Stephan A, Barrot M, Cassel J-C, Dupont J-L, Doussau F, Poulain B, Selimi F, Léna C, Isope P**. Clusters of cerebellar Purkinje cells control their afferent climbing fiber discharge. *Proc. Natl. Acad. Sci. U.S.A.* 110: 16223–16228, 2013. doi: 10.1073/pnas.1302310110.
20. **Chen X, Kovalchuk Y, Adelsberger H, Henning H, Sausbier M, Wietzorrek G, Ruth P, Yarom Y, Konnerth A**. Disruption of the olivo-cerebellar circuit by Purkinje neuron-specific ablation of BK channels. *Proc. Natl. Acad. Sci. U.S.A.* 107: 12323–12328, 2010. doi: 10.1073/pnas.1001745107.
21. **Clopath C, Badura A, De Zeeuw C, Brunel N**. A Cerebellar Learning Model of Vestibulo-Ocular Reflex Adaptation in Wild-Type and Mutant Mice. *J. Neurosci* 34: 7203-7215, 2014. doi: 10.1523/JNEUROSCI.2791-13.2014.
22. **Coesmans M, Weber JT, De Zeeuw C, Hansel C**. Bidirectional parallel fiber plasticity in the cerebellum under climbing fiber control. *Neuron*, 44(4): 691-700, 2004. doi: 10.1016/j.neuron.2004.10.031.

23. **D'Angelo E, De Zeeuw C**. Timing and plasticity in the cerebellum: focus on the granular layer. *Trends in neurosciences,* 32:30-40, 2009. doi: 10.1016/j.tins.2008.09.007.
24. **Dean P, Porrill J**. The cerebellum as an adaptive filter: a general model?. *Functional neurology*, 25:173-180, 2010.
25. **De Zeeuw C, Berrebi AS**. Postsynaptic targets of Purkinje cell terminals in the cerebellar and vestibular nuclei of the rat. *European Journal of Neuroscience* 7: 2322–33, 1995. doi:10.1111/j.1460-9568.1995.tb00653.x.
26. **De Zeeuw C, Gerrits N, Voogd J, Leonard C, Simpson J**. The rostral dorsal cap and ventrolateral outgrowth of the rabbit inferior olive receive a GABAergic input from dorsal group Y and the ventral dentate nucleus. *J. Comp. Neurol.* 341: 420–432, 1994.
27. **Dietrichs E, Walberg F**. The cerebellar corticonuclear and nucleocortical projections in the cat as studied with anterograde and retrograde transport of horseradish peroxidase. I. The paramedian lobule. *Anat. Embryol.* 158: 13–39, 1979.
28. **Dieudonné S**. Glycinergic synaptic currents in Golgi cells of the rat cerebellum. *Proceedings of the National Academy of Sciences* 92: 1441–1445, 1995. doi: 10.1073/pnas.92.5.1441.
29. **Dieudonné S**. Submillisecond kinetics and low efficacy of parallel fibre-Golgi cell synaptic currents in the rat cerebellum. *J phys*, 510: 845-866 ,1998. doi: 10.1111/j.1469-7793.1998.845bj.x.
30. **Dijck G, Hulle M, Heiney S, Blazquez P, Meng H, Angelaki D, Arenz A, Margrie T, Mostofi A, Edgley S, Bengtsson F, Ekerot C-F, Jörntell H, Dalley J, Holtzman T**. Probabilistic Identification of Cerebellar Cortical Neurones across Species. *PLoS ONE* 8, 2013. doi: 10.1371/journal.pone.0057669.
31. **Dugué G, Brunel N, Hakim V, Schwartz E, Chat M, Lévesque M, Courtemanche R, Léna C, Dieudonné S**. Electrical Coupling Mediates Tunable Low-Frequency Oscillations and Resonance in the Cerebellar Golgi Cell Network. *Neuron* 61: 126-139, 2009. doi: 10.1016/j.neuron.2008.11.028.
32. **Dumoulin A, Triller A, Dieudonné S**. IPSC kinetics at identified GABAergic and mixed GABAergic and glycinergic synapses onto cerebellar Golgi cells. *J. Neurosci,* 21: 6045-6057, 2001.
33. **Fredette B, Mugnaini E**. The GABAergic cerebello-olivary projection in the rat. *Anat. Embryol.* 184: 225–43, 1991.
34. **Gao H, Solages C, Lena C**. Tetrode recordings in the cerebellar cortex. *J. Physiol. Paris* 106: 128–36, 2011. doi: 10.1016/j.jphysparis.2011.10.005.
35. **Gauck V, Jaeger D**. The control of rate and timing of spikes in the deep cerebellar nuclei by inhibition. *J Neurosci*, 20: 3006-3016, 2000.
36. **Gould BB, Graybiel AM**. Afferents to the cerebellar cortex in the cat: evidence for an intrinsic pathway leading from the deep nuclei to the cortex. *Brain research,* 100: 601-611, 2004. doi:10.1016/0006-8993(76)90869-6.
37. **Gould B**. The organization of afferents to the cerebellar cortex in the cat: Projections from the deep cerebellar nuclei. *J. Comp. Neurol.* 184: 27–42, 1979. doi: 10.1002/cne.901840103.
38. **Haines DE, Manto MU**. The discovery and definitive proof of cerebellar nucleocortical projections 1976. *Cerebellum,* 8:1-18, 2009. doi: 10.1007/s12311-008-0054-8.
39. **Haines D, Pearson J**. Cerebellar corticonuclear – nucleocortical topography: A study of the tree shrew (Tupaia) paraflocculus. *J. Comp. Neurol.* 187: 745–758, 1979. doi: 10.1002/cne.901870407.
40. **Haines D**. Evidence of intracerebellar collateralization of nucleocortical cell processes in a prosimian primate (Galago): A fluorescence retrograde study. *J. Comp. Neurol.* 275: 441–451, 1988. doi: 10.1002/cne.902750308.
41. **Hansel C, Linden DJ**. Long-term depression of the cerebellar climbing fiber–Purkinje neuron synapse. *Neuron* 26: 473–482, 2000. doi:10.1016/S0896-6273(00)81179-4
42. **Heck DH, Thach WT**. On-beam synchrony in the cerebellum as the mechanism for the timing and coordination of movement. *PNAS,* 104:7658-7663, 2007. doi: 10.1073/pnas.0609966104
43. **Holtzman T, Rajapaksa T, Mostofi A, Edgley SA.** Different responses of rat cerebellar Purkinje cells and Golgi cells evoked by widespread convergent sensory inputs. *J. Physiol* 574: 491–507, 2006. doi: 10.1113/jphysiol.2006.108282
44. **Houck BD, Person AL**. Cerebellar premotor output neurons collateralize to innervate the cerebellar cortex. *J Comp Neurol* , accepted article, 2015. doi: 10.1002/cne.23787.
45. **Houck B, Person A**. Cerebellar Loops: A Review of the Nucleocortical Pathway. *Cerebellum* 13: 378–385, 2013. doi: 10.1007/s12311-013-0543-2
46. **Huang S, Uusisaari M**. Physiological temperature during brain slicing enhances the quality of acute slice preparations. *Front Cell Neurosci* 7: 48, 2013. 10.3389/fncel.2013.00048

47. **Hull C, Chu Y, Thanawala M, Regehr W**. Hyperpolarization Induces a Long-Term Increase in the Spontaneous Firing Rate of Cerebellar Golgi Cells. *J Neurosci* 33: 5895–5902, 2013. doi: 0.1523/JNEUROSCI.4052-12.2013
48. **Hull C, Regehr W**. Identification of an Inhibitory Circuit that Regulates Cerebellar Golgi Cell Activity. *Neuron* 73, 2011. doi: 10.1016/j.neuron.2011.10.030
49. **Husson Z, Rousseau C, Broll I, Zeilhofer H, Dieudonné S**. Differential GABAergic and Glycinergic Inputs of Inhibitory Interneurons and Purkinje Cells to Principal Cells of the Cerebellar Nuclei. *J Neurosci* 34: 9418–9431, 2014. doi: 10.1523/JNEUROSCI.0401-14.2014
50. **Hámori J, Somogyi J**. Differentiation of cerebellar mossy fiber synapses in the rat: a quantitative electron microscope study. *J Comp Neurol* 220:365-377, 1983. doi: 10.1002/cne.902200402.
51. **Hámori J, Mezey É, Szentágothai J**. Electron microscopic identification of cerebellar nucleocortical mossy terminals in the rat. *Exp Brain Res* 44, 1980. doi: 10.1007/BF00238753
52. **Hámori J, Takács J**. Two types of GABA-containing axon terminals in cerebellar glomeruli of cat: An immunogold-EM study. *Exp Brain Res* 74, 1988.
53. **Ito M**. Movement and thought: identical control mechanisms by the cerebellum. *Trends Neurosci.* 16: 448–50; discussion 453–4, 1993. doi:10.1016/0166-2236(93)90073-U
54. **Jacobson G, Rokni D, Yarom Y**. A model of the olivo-cerebellar system as a temporal pattern generator. *Trends Neurosci.* 31: 617–25, 2008. doi:10.1016/j.tins.2008.09.005
55. **Jakab RL, Hamori J**. Quantitative morphology and synaptology of cerebellar glomeruli in the rat. *Anat embryol* 179: 81-88. doi: 10.1007/BF00305102
56. **Kanichay R, Silver R.** Synaptic and cellular properties of the feedforward inhibitory circuit within the input layer of the cerebellar cortex. J Neurosci 28: 8955–67, 2008. doi: 10.1523/JNEUROSCI.5469-07.2008
57. **Korbo L, Andersen BB, Ladefoged O, Møller A**. Total numbers of various cell types in rat cerebellar cortex estimated using an unbiased stereological method. *Brain Res.* 609: 262–8, 1993. doi:10.1016/0006-8993(93)90881-M
58. **Lefler Y, Yarom Y, Uusisaari M**. Cerebellar Inhibitory Input to the Inferior Olive Decreases Electrical Coupling and Blocks Subthreshold Oscillations. *Neuron* 81, 2014. doi: 10.1016/j.neuron.2014.02.032
59. **Legendre A, Courville J**. Cerebellar nucleocortical projection with a survey of factors affecting the transport of radioactive tracers. *J. Comp. Neurol.* 252: 392–403, 1986. doi: 10.1002/cne.902520308
60. **Leiner HC, Leiner AL, Dow RS**. Cognitive and language functions of the human cerebellum. *Trends Neurosci* 16: 444–447, 1993. doi:10.1016/0166-2236(93)90072-T
61. **Longley M, Yeo C**. Distribution of neural plasticity in cerebellum-dependent motor learning. *Prog. Brain Res.* 210: 79–101, 2014. doi: 10.1016/B978-0-444-63356-9.00004-2
62. **Medina JF, Lisberger SG**. Links from complex spikes to local plasticity and motor learning in the cerebellum of awake-behaving monkeys. *Nat Neurosci* 11, 1185 - 1192, 2008. doi:10.1038/nn.2197
63. **Najac M, Raman IM**. Integration of Purkinje Cell Inhibition by Cerebellar Nucleo-Olivary Neurons. *J. Neurosci. 35: 544–9, 2015*. doi: 10.1523/JNEUROSCI.3583-14.2015.
64. **Ottersen OP, Storm-Mathisen J, Somogyi P**. Colocalization of glycine-like and GABA-like immunoreactivities in Golgi cell terminals in the rat cerebellum: a postembedding light and electron microscopic study. *Brain Res.* 450: 342–53, 1988.
65. **Payne J**. The cerebellar nucleo-cortical projection in the rat studied by the retrograde fluorescent double-labelling method. *Brain Res* 271: 141144, 1983. doi: 10.1016/0006-8993(83)91374-4
66. **Pedroarena CM, Schwarz C**. Efficacy and short-term plasticity at GABAergic synapses between Purkinje and cerebellar nuclei neurons *J neurophysiol* 89: 704–15, 2003. doi: 10.1152/jn.00558.2002
67. **Person AL, Raman IM.** Purkinje neuron synchrony elicits time-locked spiking in the cerebellar nuclei. Nature 481: 502–5, 2012**.** doi: 10.1038/nature10732
68. **Pietrajtis K, Dieudonné S**. Golgi Neurons. *In:* Handbook of the cerebellum and cerebellar disorders, *Springer,* 2013. doi: 10.1007/978-94-007-1333-8_34.
69. **Pijpers A, Voogd J, Ruigrok T**. Topography of olivo-cortico-nuclear modules in the intermediate cerebellum of the rat. *J Comp. Neurol.* 492: 193-213, 2005. doi: 10.1002/cne.20707.
70. **Provini L, Marcotti W, Morara S, Rosina A**. Somatotopic nucleocortical projections to the multiple somatosensory cerebellar maps. *Neuroscience* 83: 1085–104, 1998.

71. **Ruigrok T, Teune TM**. Collateralization of cerebellar output to functionally distinct brainstem areas. A retrograde, non-fluorescent tracing study in the rat *Front Syst Neurosci* 8: 23, 2014. doi: 10.3389/fnsys.2014.00023
72. **Ruigrok T**. Ins and Outs of Cerebellar Modules. *Cerebellum* 10: 464–474, 2010. doi:10.1007/s12311-010-0164-y
73. **Schindelin J, Arganda-Carreras I, Frise E, Kaynig V, Longair M, Pietzsch T, Preibisch S, Rueden C, Saalfeld S, Schmid B, Tinevez J-Y, White D, Hartenstein V, Eliceiri K, Tomancak P, Cardona A**. Fiji: an open-source platform for biological-image analysis. *Nat Meth* 9: 676–682, 2012. doi: 10.1038/nmeth.2019
74. **Schneider DM, Nelson A, Mooney R**. A synaptic and circuit basis for corollary discharge in the auditory cortex *Nature* 513: 189–94, 2014. doi: 10.1038/nature13724
75. **Schulman JA, Bloom FE**. Golgi cells of the cerebellum are inhibited by inferior olive activity. *Brain Res* 210: 350–5, 1981. doi: 10.1016/0006-8993(81)90908-2
76. **Simat M, Parpan F, Fritschy J-MM**. Heterogeneity of glycinergic and gabaergic interneurons in the granule cell layer of mouse cerebellum. *J. Comp. Neurol.* 500: 71–83, 2007. doi: 10.1002/cne.21142
77. **Sommer MA, Wurtz RH**. Brain circuits for the internal monitoring of movements *Ann. rev. neurosci* 31:37, 2008. doi: 10.1146/annurev.neuro.31.060407.125627.
78. **Sultan F, Augath M, Hamodeh S, Murayama Y**. Unravelling cerebellar pathways with high temporal precision targeting motor and extensive sensory and parietal networks. *Nat comm* 3: 924, 2012. doi: 10.1038/ncomms1912
79. **Taniguchi H, He M, Wu P, Kim S, Paik R, Sugino K, Kvitsiani D, Kvitsani D, Fu Y, Lu J, Lin Y, Miyoshi G, Shima Y, Fishell G, Nelson S, Huang Z**. A Resource of Cre Driver Lines for Genetic Targeting of GABAergic Neurons in Cerebral Cortex. *Neuron* 71, 2011. doi: 10.1016/j.neuron.2011.07.026
80. **Telgkamp P, Padgett D, Ledoux V, Woolley C, Raman I.** Maintenance of high-frequency transmission at purkinje to cerebellar nuclear synapses by spillover from boutons with multiple release sites. *Neuron* 41: 113–26, 2004.
81. **Telgkamp P, Raman I.** Depression of inhibitory synaptic transmission between Purkinje cells and neurons of the cerebellar nuclei. *J Neurosci* 22: 8447–57, 2002.
82. **Teune TM, Burg J, De Zeeuw C, Voogd J, Ruigrok TJH.** Single Purkinje cell can innervate multiple classes of projection neurons in the cerebellar nuclei of the rat: A light microscopic and ultrastructural triple-tracer study in the rat. *J. Comp. Neurol*. 392: 164–178, 1998. doi: 10.1002 (SICI)1096-9861(19980309)392:2<164::AID-CNE2>3.0.CO;2-0
83. **Thompson R, Steinmetz J**. The role of the cerebellum in classical conditioning of discrete behavioral responses. *Neuroscience* 162: 732–55, 2009. doi:10.1016/j.neuroscience.2009.01.041
84. **Tolbert D, Kultas-Ilinsky K, Ilinsky I**. EM-autoradiography of cerebellar nucleocortical terminals in the cat. *Anat. and embryol.* 161: 215-223, 1980. doi: 10.1007/BF00305345.
85. **Tolbert DL, Bantli H, Bloedel JR**. Anatomical and physiological evidence for a cerebellar nucleo-cortical projection in the cat. *Neuroscience 1: 205–17, 1976*. doi:10.1016/0306-4522(76)90078-6.
86. **Tolbert D, Bantli H, Bloedel J**. The intracerebellar nucleocortical projection in a primate. *Exp Brain Res* 30-30, 1977. doi: 10.1007/BF00237266
87. **Tolbert D, Bantli H, Bloedel J**. Organizational features of the cat and monkey cerebellar nucleocortical projection. *J. Comp. Neurol.* 182: 39–56, 1978. doi:10.1002/cne.901820104
88. **Tolbert D, Bantli H**. An HRP and autoradiographic study of cerebellar corticonuclear-nucleocortical reciprocity in the monkey. *Exp Brain Res* 36:563-571, 1979. doi:10.1007/BF00238523
89. **Tsukahara N, Bando T**. Red nuclear and interposate nuclear excitation of pontine nuclear cells. *Brain research* 19: 295–298, 1970. doi:10.1016/0006-8993(70)90442-7
90. **Uusisaari M, Knöpfel T**. GlyT2+ neurons in the lateral cerebellar nucleus. *The Cerebellum* 9: 42–55, 2010. doi 10.1007/s12311-009-0137-1
91. **Uusisaari MY, Knöpfel T**. Diversity of neuronal elements and circuitry in the cerebellar nuclei. *The Cerebellum* 11: 420–1, 2012. doi: 10.1007/s12311-011-0350-6.
92. **Vervaeke K, Lőrincz A, Gleeson P, Farinella M, Nusser Z, Silver R**. Rapid Desynchronization of an Electrically Coupled Interneuron Network with Sparse Excitatory Synaptic Input. *Neuron* 67, 2010. doi:10.1016/j.neuron.2010.06.028

93. **Vos B, Volny-Luraghi A, Schutter E**. Cerebellar Golgi cells in the rat: receptive fields and timing of responses to facial stimulation. *Eur. J. Neurosci.* 11: 2621–2634, 1999. doi: 10.1046/j.1460-9568.1999.00678.x
94. **Wilms CD, Häusser M**. Reading out a spatiotemporal population code by imaging neighbouring parallel fibre axons in vivo. *Nature communications* 6:6464, 2015. doi: 10.1038/ncomms7464.
95. **Xu W, Edgley S**. Climbing fibre-dependent changes in Golgi cell responses to peripheral stimulation. *J. Physiol. (Lond.)* 586: 4951–4959, 2008.
96. **Zeilhofer H, Studler B, Arabadzisz D, Schweizer C, Ahmadi S, Layh B, Bösl M, Fritschy J**. Glycinergic neurons expressing enhanced green fluorescent protein in bacterial artificial chromosome transgenic mice. *J. Comp. Neurol.* 482: 123–141, 2005.

957 **FIGURES**

958 **Figure 1. Targeted viral labeling of the GABAergic and glycinergic neurons in the CN reveal dense**
959 **and wide-spread network of nucleo-cortical axons in the cerebellar cortex. A1-B1**. Confocal images
960 of coronal cerebellar sections in mice where floxed virus was injected into the cerebellar nuclei of GAD-cre
961 and GlyT2-cre mice. **A1,** flocculus, coronal view, 40x confocal scan tiles. **B1,** posterior vermis, horizontal
962 view **A2**-**B2**. Higher magnification confocal images of the cerebellar nuclei show transfected GABAergic
963 and glycinergic neurons, respectively. Note the lower density of labeled neurons in GlyT2-cre brain. In the
964 GAD-cre mice, both small, globular and larger, multipolar neurons (arrows and arrowheads in **A2**, respec-
965 tively) were seen. In the GlyT2-cre mice, only large, multipolar neurons were observed, characteristic to
966 the glycinergic CN neurons (arrowheads in **B2**). In the GAD-cre mice the transfected neurons included the
967 GABAergic NO neurons, as evidenced by the fluorescent axons in the contralateral IO (**A3**). **C**. Injection of
968 hSyn-GFP-virus into the inferior olive retrogradely labelled small, round NO neurons in the contralateral
969 CN. **D**. Comparison of soma sizes among the three labeled populations. The histograms are fitted with
970 single (GlyT2+ and NO) or double (GAD+) gaussians (thick lines), showing that the GlyT2+ neurons distri-
971 bution matches the second peak in GAD+ fit and that the GlyT2+ and NO neurons form distinct popula-
972 tions that contribute to the GAD+ population. **E**. Confocal composite images showing virally transfected CN
973 neurons in GAD-cre (**E1**) and GlyT2-cre (**E2**) mice, and their axons (arrows) extending across the white
974 matter (WM) surrounding the CN into the granule cell layer (GrCL) of the cerebellar cortex. **F1**. Confocal
975 composite image of a caudal coronal section of GlyT2-cre cerebellum where the lateral CN was virally
976 transfected (location of the CN is drawn schematically on top of the image). The wide distribution of the
977 NC axons in medio-lateral direction, including parts of the contralateral cerebellum, is shown in yellow
978 color. **F2**. Confocal composite image of a horizontal section at the level of the CN in GlyT2-cre cerebellum
979 with transfection of the glycinergic neurons in the medial CN. The axons of the labeled neurons can be
980 seen extending through wide areas of the vermal cortex. The inset shows a single iNC axon forming axonal
981 swellings across several hundreds of μm in the GrCL. Abbreviations: GrCL, granule cell layer; CN, cerebel-
982 lar nuclei; mCN, medial cerebellar nuclei; IO, inferior oive; NO, nucleo-olivary; WM, white matter. Scale
983 bars: A1, B1: 50 μm; A2, B2, C, 10 μm; E, 100 μm, F, G: 400 μm; G, inset: 100 μm. See also figure supple-
984 ment 1.

985

986 **Figure 1–figure supplement 1. iNC neurons receive functional GABAergic Purkinje Neuron inputs.**
987 **A.** In the GlyT2-eGFP mouse, GFP – positive neurons (in green) are contacted by VIAAT - positive
988 varicosities (in red). Points of contacts are indicated by arrows. (Z-projection thickness: 4.6 μm, scale bar:
989 10 μm). **B.** Optogenetical stimulation of Purkinje neurons axonal varicosities were performed by whole
990 field LED (470 nm) illumination of the cerebellar nuclei of L7-ChR2-YFP mice bred with GlyT2-eGFP mice.
991 In these double-positive mice, Purkinje neurons expressed specifically the ChR2 (Chaumont et al., 2014)
992 while iNC neurons can be easily targeted for patch-clamp recording using epifluorescence for GlyT2-eGFP.
993 **C.** One millisecond illumination (indicated by blue box) elicited large inhibitory responses in the iNC
994 neurons (mean amplitude of 416.5 ± 332.1 pA, n = 10 cells), in presence of glutamate receptors blockers
995 (APV 50 μM, NBQX 10 μM), which were blocked by 1 μM gabazine (98.1 ± 1.4 % block, n = 9 cells). The
996 kinetics of the PN-originating IPSCs in glycinergic CN cells (decay time constant 3.28 ± 0.72 ms, n = 10
997 cells) were similar to those of IPSCs at Purkinje cell synapses on glutamatergic projection neurons
998 (Telgkamp and Raman, 2002; Person and Raman 2012; Husson et al, 2014; Kawaguchi and Sakaba, 2015)
999 but much faster than at Purkinje cell synapses on NO cells (Najac and Raman, 2015), suggesting
1000 differential control of the GABAergic NO cells and the larger, GABA-glycinergic CN cells by PNs.

1001

1002 **Figure 2. iNC axons are found in cerebellar granule cell and molecular layers and contain GAD65-**
1003 **67 and GlyT2. A-B**. Confocal composite images of sections through the flocculus in GAD-cre (**A1**) and
1004 posterior vermis in GlyT2-cre (**B1**) mice, showing dense iNC axons in the GrCl as well as sparse axons in
1005 the ML (arrows). 40x composite tiles. Large axonal swellings from both GABAergic (**A2**) and glycinergic
1006 (**B2**) axons are found in the GrCL. Both GABAergic (**A3**) and glycinergic (**B3**) iNC axons occasionally rise
1007 into the lower ML. **C**. Comparison of iNC axonal bouton sizes between the GABAergic and glycinergic axons
1008 (**C1**) and between the boutons in the GrCL and ML (**C2**) shows nearly identical distributions. **D**. Merged
1009 confocal image (Z-projection thickness: 12.2 μm) showing iNC axons in GAD-cre mice injected with AAV-
1010 flox-EYFP (green) are co-stained for GlyT2 (red) (**D1**). Higher magnification of axonal swellings (arrows)
1011 co-stained for EYFP and GlyT2 (**D2**). **E**. iNC boutons (green) transfected with AAV-flox-EYFP in GlyT2-cre
1012 mice are stained for GAD65-67 (red, **E1**, Z-projection thickness: 8.2 μm). (**E2**) Higher magnification of iNC
1013 axon (arrows) co-stained for EYFP and GAD65-77 (Z-projection thickness: 2.4 μm). Abbreviations: GrCL,
1014 granule cell layer; ML, molecular layer; PNL, Purkinje neuron layer; WM, white matter; n.s., non-
1015 significant. Scale bars: A1 and B1: 100 μm; A2 and B2: 5 μm; A3 and B3: 50 μm. D1: 20 μm. D2-4: 5 μm.
1016 E1a-e: 10 μm; E2a-e: 2 μm.

1017

1018 **Figure 3. Optogenetic stimulation of iNC axons in cerebellar slices inhibits Golgi cells' spiking.**

1019 **A.** Confocal image (left) and reconstruction (right) of GrCL in GAD-cre mouse injected with AAV2-flox-
1020 ChR2-mCherry to the CN and AAV-GFP to the cerebellar cortex. iNC fibers (red) branch in the GrCL and
1021 form axonal swellings (arrows) on GoCs (green). **B**, Left: Schematic drawing of the *in vitro* experimental
1022 arrangement. GoCs were recorded in GlyT2-cre or GAD-cre animals where iNC axons express both ChR2
1023 and a fluorescent marker (YFP in GlyT2-cre, mCherry in GAD-cre). Right: GoC patched and filled with Neu-
1024 robiotin (green) in GlyT2-Cre mice surrounded by transfected axons (red) (Z-projection thickness: 36.4
1025 μm; Sagittal view). **C.** Optogenetic stimulation of the iNC fibers. **C1.** An example of averaged IPSCs (n = 30)
1026 recorded in Golgi cell induced by 5 ms illumination (indicated by blue line), blocked by successive bath
1027 application of 300 nM strychnine (str; orange) and 2 μM gabazine (gbz, blue). **C2.** Summary plot of the
1028 percentage of inhibitory current blocked by strychnine and gabazine (n = 9; p = 0.0039). **D.** Example volt-
1029 age traces from a recorded Golgi cell with a 50 ms single light pulse in GAD-Cre mice. The averaged IPSP
1030 response (± STD) of all 6 traces is magnified in the inset. **E.** iNC activation delays spike generation in GoCs.
1031 **E1.** The traces recorded without (top; ctrl; black) and with (bottom; stim; blue) light stimulation are
1032 aligned either on the first spike in the sweep (top) or on the spike preceding the stimulus (bottom; red,
1033 dashed line) to emphasize the increased ISI in response to iNC stimulation. Average inhibition delay (±
1034 STD) for the example cell is marked above traces in Box-and-whiskers symbols. **E2.** Comparison of the
1035 average ISI without and with light pulse (± STD) normalized to the average ISI. (p = 0.0001; n = 15). **F.**
1036 Example voltage traces from a recorded GoC during train of light pulses stimulation of iNC axons showing
1037 no spikes occurring during the illumination (upper panel). PSTH of the GoCs (n = 16, 100 ms bin) shows a
1038 decrease in the number of spikes after train pulse stimulation. Baseline average marked in dashed red line
1039 and STD values in red area (all cells normalized to baseline frequency; lower panel). Scale bars: A. 20 μm,
1040 B. 50 μm. Asterisks indicates statistical significance. Abbreviations: WM, white matter; GrCL, granule cell
1041 layer; GoC, Golgi cell; ML, molecular layer; ISI, inter-spike interval. See also figure supplement 1.

1042 **Figure 3 –figure supplement 1. iNC activation modulate spike times in a fraction of non-responsive**
1043 **s-Golgi cells. A**. An example Golgi cell current clamp recording showing spike-timing response to train of
1044 light pulses (upper panel, 6 traces). Spike-timing analysis shows a significant decrease in the voltage
1045 variability between the different recorded traces (bottom panel; red dashed line indicate z-score = 3, p=
1046 0.05). **B**. Population spike-timing analysis showing a decrease in the voltage variability in GoCs after
1047 optogenetic stimulation of iNC fibers (n = 7; p = 0.05). Black dots above traces mark spike times.

1048

1049 **Figure 4. Golgi cell subtypes differ in their sensitivity to iNC input and have different intrinsic**
1050 **properties**. **A**, left: A spontaneously active GoC (s-GoC) is inhibited by optogenetic iNC activation (light-
1051 blue bars above traces). Six superimposed traces with no holding current. **A**, right: A not-spontaneously
1052 spiking GoC (ns-GoCs) shows no response to iNC activation. Bottom trace: without depolarizing current
1053 injection; top trace: with +8 pA current injection to evoke spiking. Black dots above traces in both panels
1054 mark spike times. **B.** Percentage and numbers of s-GoCs (blue) and ns-GoCs (green) that are inhibited by
1055 iNC axons (left) and those that are not (right). **C.** Example traces of three GoCs' responses to positive cur-
1056 rent steps. Cell 1, blue: s-GoC (C_m = 173.5 pF); Cell 2, dark green: a large ns-GoC (C_m = 125.3 pF); Cell 3,
1057 light green: small ns-GoC (C_m = 73.0 pF). **D**. AP waveforms differ between s-GoCs and ns-GoCs. Left: super-
1058 imposed, grand average action potential shapes (± STD) obtained from s-GoCs (n = 31 cells, blue) and ns-
1059 GoCs (n = 13 cells, green) during steady-state firing. Right: APs are peak-normalized (± SEM). s-GoCs show
1060 faster spike repolarization as well as faster after-hyperpolarization (arrowhead). **E.** Comparison of AP
1061 parameters shows that s-GoCs (n = 31 cells) spikes are faster than those in ns-GoCs (n = 13 cells). **F.** Cur-
1062 rent-to-firing frequency (IF) relationship of s-GoCs (blue, n = 23) and ns-GoCs (green, n = 11) are not sig-
1063 nificantly different. The solid and dashed lines show fitted single polynomials and the confidence inter-
1064 vals, respectively. The current injection values are normalized to the estimated C_m of the cells. **G.** C_m and
1065 input resistance of s-GoCs (blue; n = 23) and ns-GoCs (green; n = 11). **H**. Comparison of instantaneous
1066 firing frequency accommodation during a depolarizing step. Left: box-plot chart showing the development
1067 of frequency accommodation in s-GoCs (blue) and ns-GoCs (green). For visual clarity, the s-GoC bars are
1068 slightly shifted to the right in respect to the ns-GoC. Right: box plots of the steady-state accommodation
1069 among s-GoCs (blue) and ns-GoCs (green) show that s-GoCs have a smaller range of accommodation than
1070 ns-GoCs (t-test, p=0.008). Asterisks denote statistical significance. Abbreviations: s-GoC, spontaneously
1071 spiking Golgi cell; ns-GoC, not spontaneously spiking Golgi cell, AP, action potential; AHP, afterhyperpolar-
1072 ization; acc val, accommodation value.
1073

1074 **Figure 5. iNC fibers contact preferentially a neurochemically distinct subtype of Golgi cells ex-**
1075 **pressing neurogranin. A-C.** iNC fibers were transfected with AAV-flox-tdTomato in GlyT2-Cre X GlyT2-
1076 eGFP mice. iNC fibers were identified in the cerebellar cortex by their co-labeling for both GFP (green) and
1077 tdTomato (red). **A-B.** In the GrCL, iNC fibers contact somata and proximal dendrites of neurogranin-
1078 expressing (blue) GoCs, either devoid of GFP staining or exhibiting a faint GFP staining at their somata
1079 (indicated by asterisks). **C**. In the ML, GFP-positive / tdTomato-positive iNC fibers (arrowheads) were also
1080 seen apposed to GoC apical dendrites stained for neurogranin (blue) and virtually devoid of GFP staining
1081 (green). **D.** iNC fibers, transfected with AAV-flox-YFP virus (green) in GAD-cre mice, contacted neu-
1082 rogranin-positive (blue) GoCs. iNC varicosities (arrowheads) are co-stained for GAD65-67 (red). **E.** Plot of
1083 the mean GlyT2-eGFP intensities over mean neurogranin intensities allows statistical discrimination (k-
1084 means 2D) between two GoCs populations**.** A first population (blue) was distinguished from the second
1085 population (green) by its none-to-low levels of GlyT2-eGFP staining, as seen with the bimodal distribution
1086 of mean GFP intensities (**F**), while the mean neurogranin intensities were less discriminative (**G**). Accord-
1087 ing to the color-coded number of iNC inputs received by each GoC (**H**), most of the "iNC-contacted" GoCs
1088 were found in the neurogranin-positive / GlyT2-eGFP negative GoC population (blue) (**I**). **J.** Schematic
1089 drawing of the percentages obtained for each GoC subtypes. Z-projection thickness: A. 34 µm; B. 18.4 µm;
1090 C. 16.3 µm; D. 30 µm; D.close up: 2.4µm. Scale bar: A. 20 µm, B-D. 10 µm, D close up: 2 µm. Abbreviation:
1091 GoC, Golgi cell.
1092

1093 **Figure 6**. **iNC neurons exhibited a burst firing phenotype and their optogenetic stimulation have**
1094 **inhibitory effects on Golgi cells firing *in vivo*. A1**. Extracellular recordings of iNC neurons in GlyT2-Cre
1095 mice transfected with ChR2 virus during increasing intensity of stimulation (1 ms duration pulse; blue
1096 bars). **A2.** iNC neurons exhibit a burst firing phenotype with increase of mean number of spikes per burst
1097 (left) and mean burst frequency (right) when increasing illumination intensity. **B1.** Whole-cell current-
1098 clamp recording of GAD-Cre iNC neurons transfected with ChR2 during 10, 50 or 200 ms long light pulse
1099 (blue bars; light intensity: 1.3 mW/mm^2) have burst firing phenotype. **B2**. GAD-Cre transfected iNC
1100 neurons show increase of their mean number of spikes per burst (left) and mean burst duration (right)
1101 with increasing illumination duration. **C1.** Schematic drawing of the experimental system for *in vivo*
1102 recordings: Extracellular recordings of GoCs during 25 ms pulse illumination of the CN in anesthetized
1103 GlyT2-Cre mice injected with ChR2 in the CN. **C2**. Raster plots of two GoCs recorded at the same time and
1104 of one PN recorded in the same area, with their corresponding peri-stimulus time histograms (PSTH).
1105 Light pulse start at 0 ms. **D1**. All superimposed smoothed PSTHs of responsive GoCs (18 out of 86
1106 recorded GoCs), normalized to their mean firing rate (FR), with the population average trace (red). Two
1107 individual traces are highlighted (orange and blue), illustrating the high variability of the inhibition period
1108 parameters. Smoothed PSTHs are obtained by convolving 1 ms time bin PSTHs with a Gaussian kernel
1109 with 3 ms standard deviation. **D2**. Characterizing parameters of the responses. **D3**. Light stimulation of
1110 iNC neurons decreased the firing rate. **D4**. Comparison of responsive and non-responsive GoCs firing rates.
1111 Abbreviations: GoC, Golgi cell.

1112

1113 **TABLES**

1114

Virus	Constructs	Mouse line and injection site	Used in Figures
AAV2/9.EF1.dflox.hChR2 (H134R)-mCherry	Addgene 20297	GAD-cre (CN)	1A, 1E1 2A 3A, 3E-I 4A-H 6B
AAV2/9.EF1a.DIO.eNpHR3.0-EYFP.WPRE.hGH	Addgene 26966	GAD-Cre (CN)	2C 5D
AAV2.1.EF1α.DIO.hChR2(H134R).eYFP	Addgene 20298	GlyT2-cre (CN)	1B, F 2B, D 3B-D 6A, C
AAV2.1.CAG-Flex.tdTomato	Allen Institute #864	GlyT2-Cre x GlyT2-eGFP (CN)	5A-C, E-F
AAV2/9.hSynapsin.EGFP.WPRE.bGH	UPenn AV-9-PV1696	GAD-cre (CN+ Cortex)	1C 3A
AAV2/9.CAG.Flex.EGFP.WPRE.bGH	Allen Institute #854	GAD-cre (CCTX)	not shown

1115
1116
1117 **Table 1. Summary of the viral constructs used.**

	Solution 1 (in MilliQ water)	Solution 2 (in Volvic water)	Solution 3 (in Volvic water)	Solution 4 (in Volvic water)	Intracellular solution
Experimental details	HUJI Cutting (33°C) and Chamber-perfusion (25-28°C) solutions	IBENS Cutting solution Ice-cold	IBENS Recovery solution 33°C	IBENS Chamber-perfusion solution (33°C)	IBENS HUJI
NaCl	124			125.7	4
K-gluconate		130			140
D-mannitol			225		
KCl	3	14.6	2.3	3.3	
Glucose	20	25	25	25	
KH_2PO_4	1.2				
NaH_2PO_4			1.25	1.25	
$MgSO_4$	3.5				
$MgCl_2$			7.7	1.17 total 1.5	
$NaHCO_3$	26		25	24.8	
$CaCl_2$	2		0.51	1.3 total 1.6	0.5
EGTA		2			5
HEPES		20			10
D-APV (µM)	20 [in recording solution]	50	50	20	
Minocycline (nM)		50	50	50	
Mg-ATP					3

1118

1119 **Table 2. Composition of solutions used for slice preparation and experiments.**

1120

	s-Golgi	ns-Golgi	N (s)	N (ns)	p-value (wilcoxon)	p-value (F-test)
AP half-width (ms)	0.8 ± 0.2	1.2 ± 0.4	33	11	0.01	0.001
AP threshold (mV)	38.9 ± 6.04	-36.4 ± 9.4	33	11	0.8	0.1
AP amplitude (mV)	51.2 ± 9	43.5 ± 10.7	33	11	0.06	0.4
AP peak voltage (mV)	22.4 ± 8.7	16.8 ± 13.03	33	11	0.1	0.17
AHP min voltage (mV)	-51.9 ± 4.5	-51.5 ± 8.8	33	11	0.8	0.01
AHP time (ms)	2.1 ± 0.8	4.0 ± 0.5	33	11	0.009	0.03
AHP amplitude (mV)	24.3 ± 4.2	23.1 ± 8.4	33	11	0.9	0.003
I-F slope (r^2)	0.5	0.4	23	11	---	0.3 (cov-analysis)
Freq. Acc. (%)	53 ± 8%	59 ± 29%	23	11	0.3	$1.1X10^{-6}$
C_m (pF)	127.5 ± 48.3	118.9 ± 78.3	23	11	0.052	0.0018
R	185.5 ± 43.2	161 ± 75.5	23	11	0.054	$8.3X10^{-5}$

1121
1122
1123 **Table 3. Summary of s-Golgi and ns-Golgi cells spiking parameters.**

1124

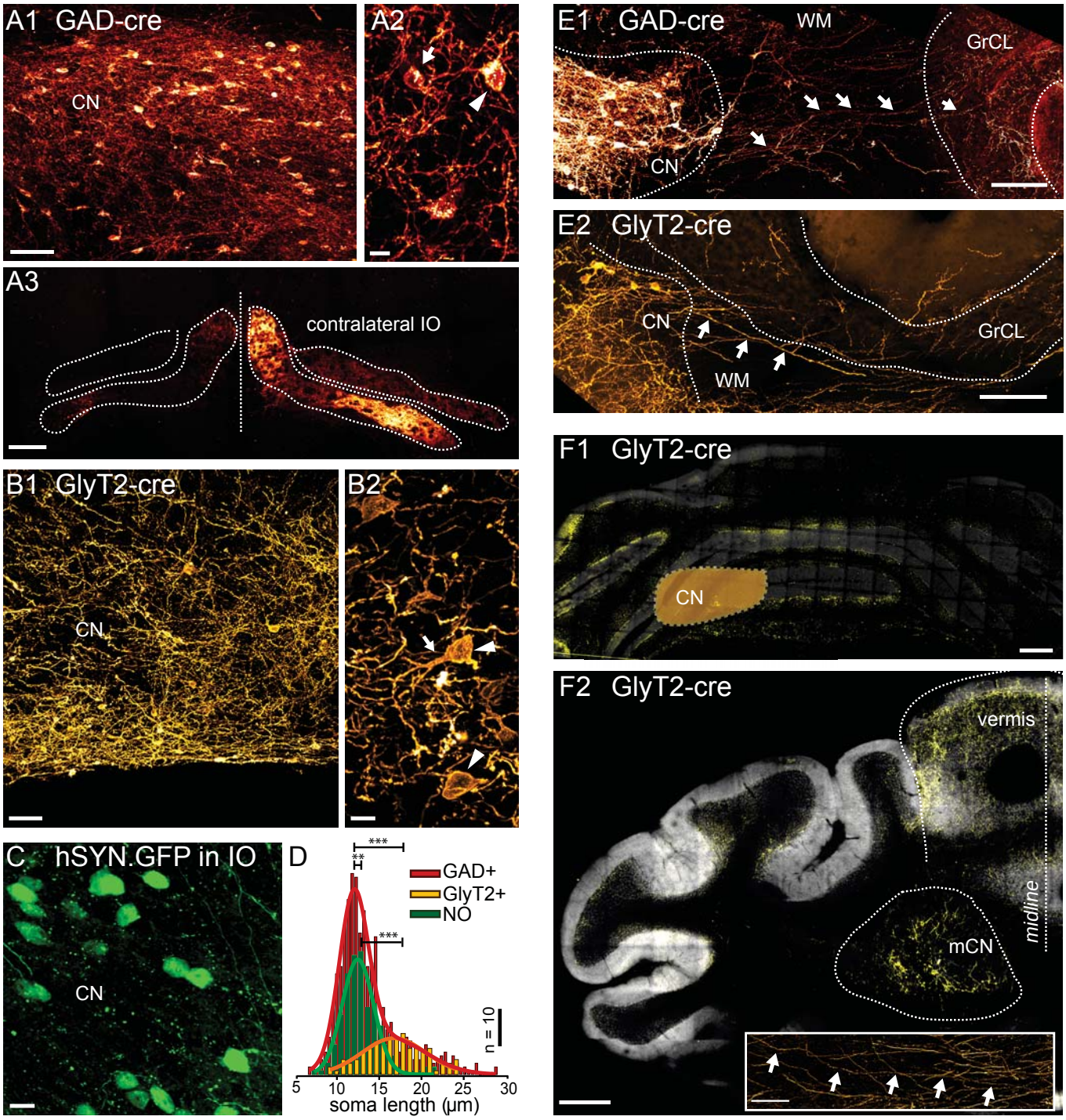

Ankri, Husson et al.
Fig 1

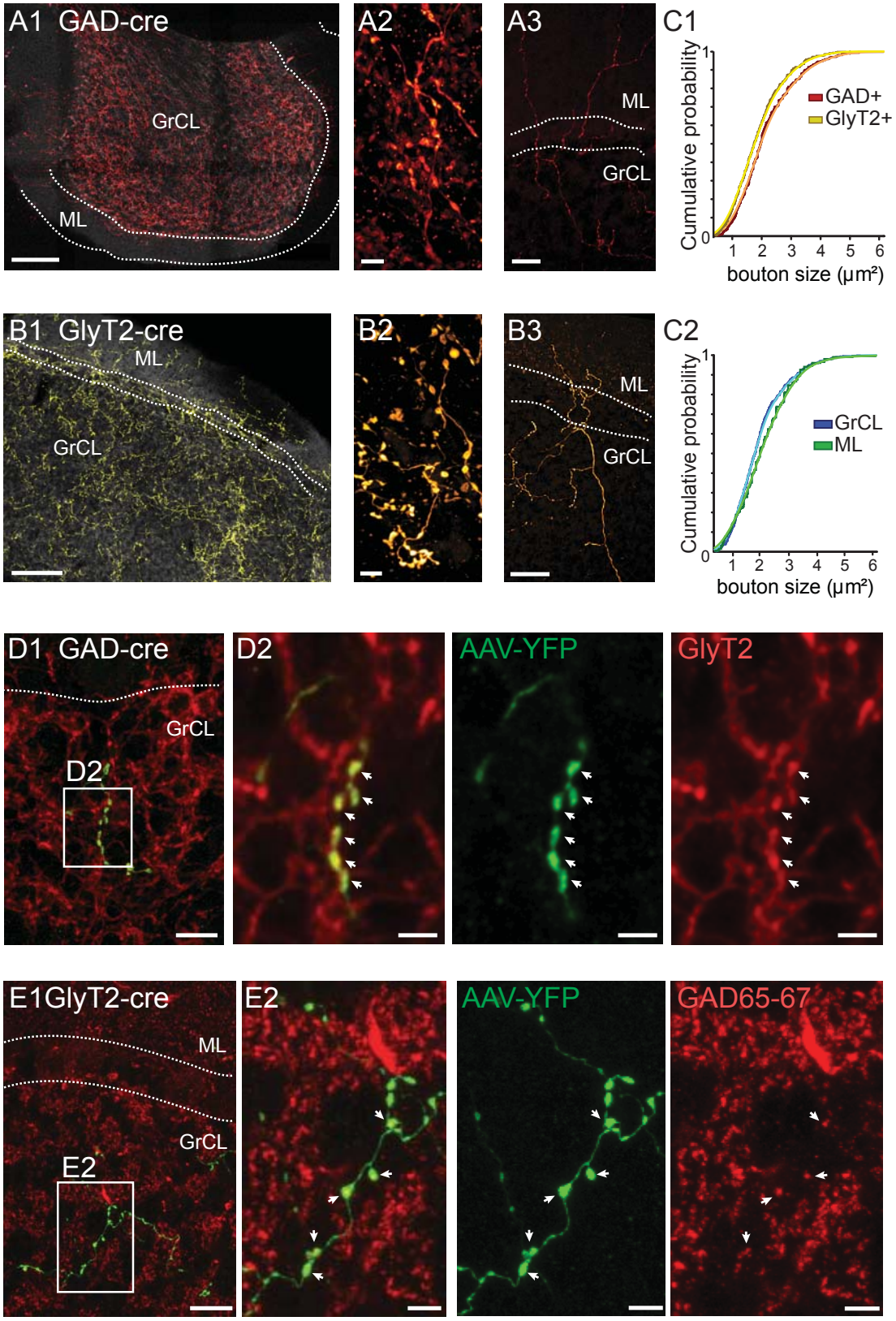

Ankri, Husson et al.
Fig 2

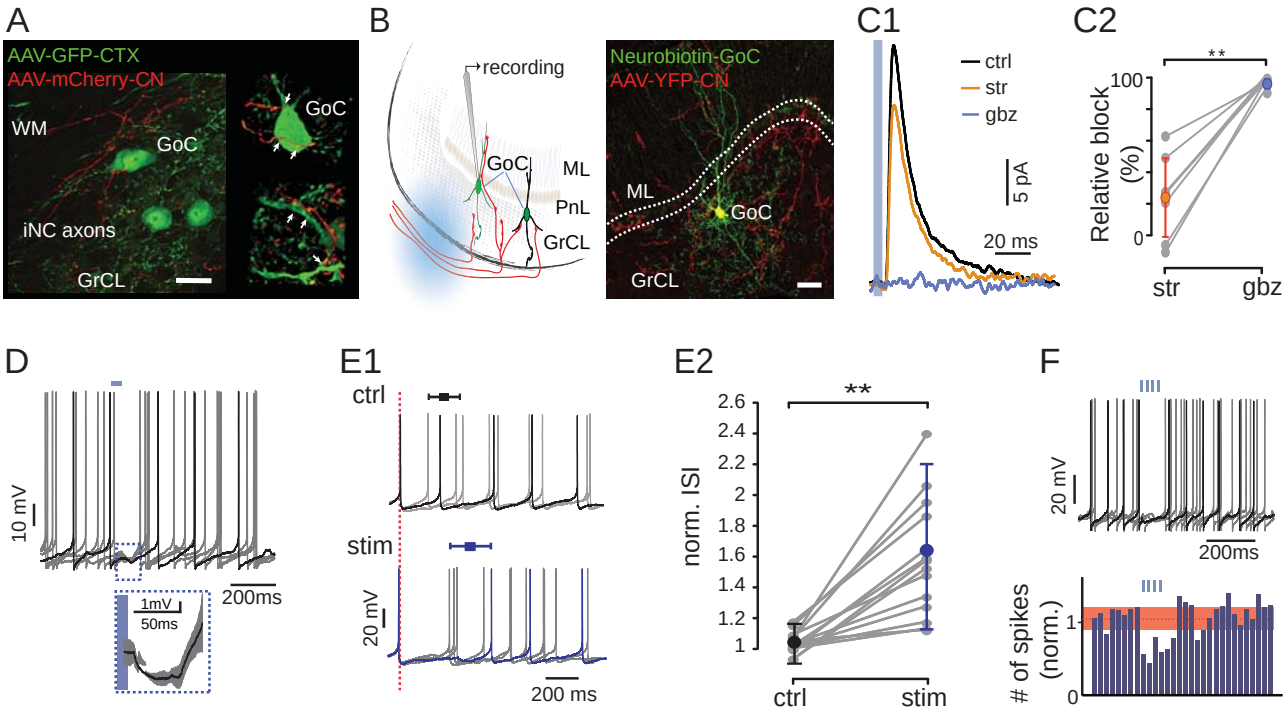

Ankri, Husson et al.
Fig 3

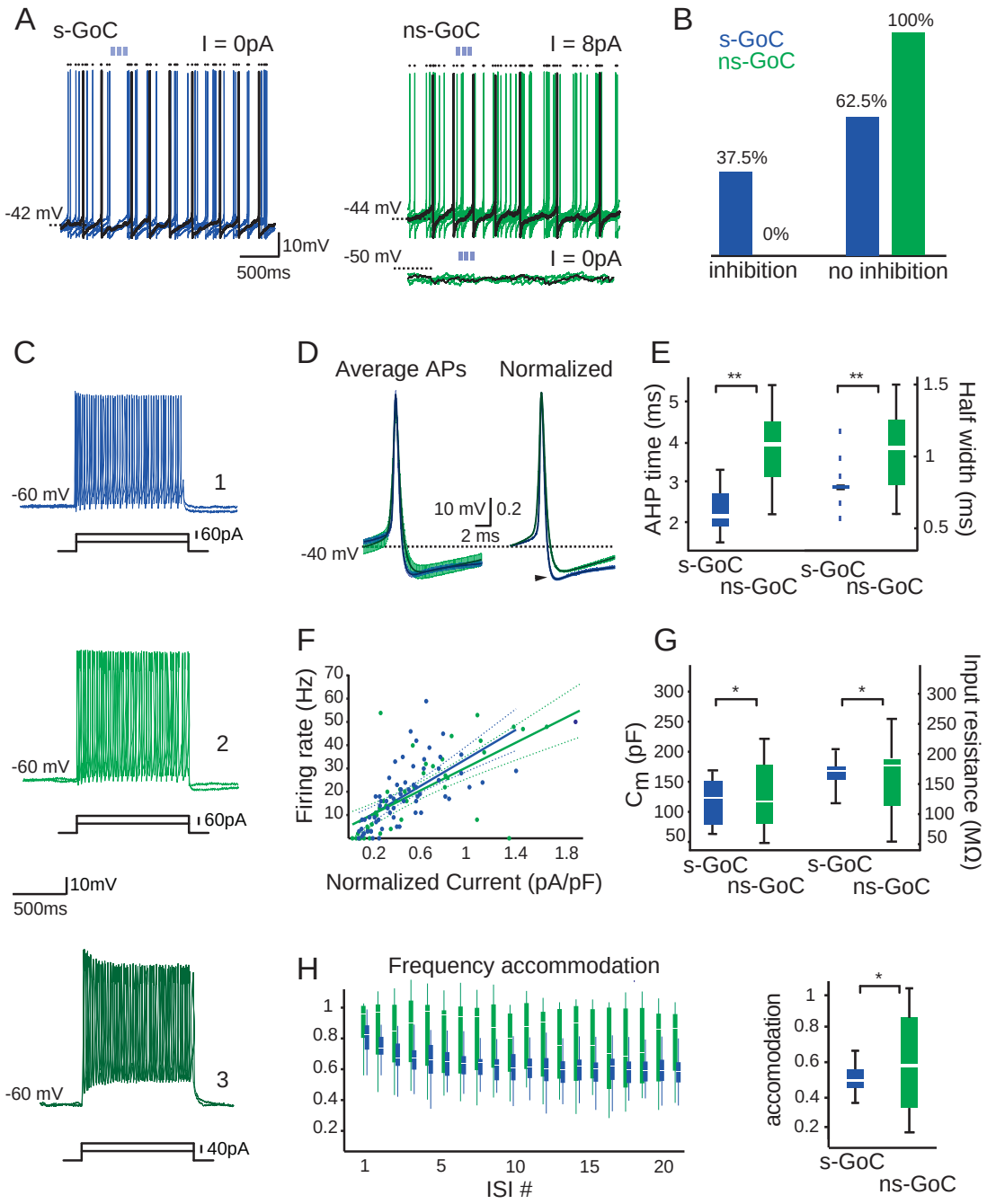

Ankri, Husson et al.
Fig. 4

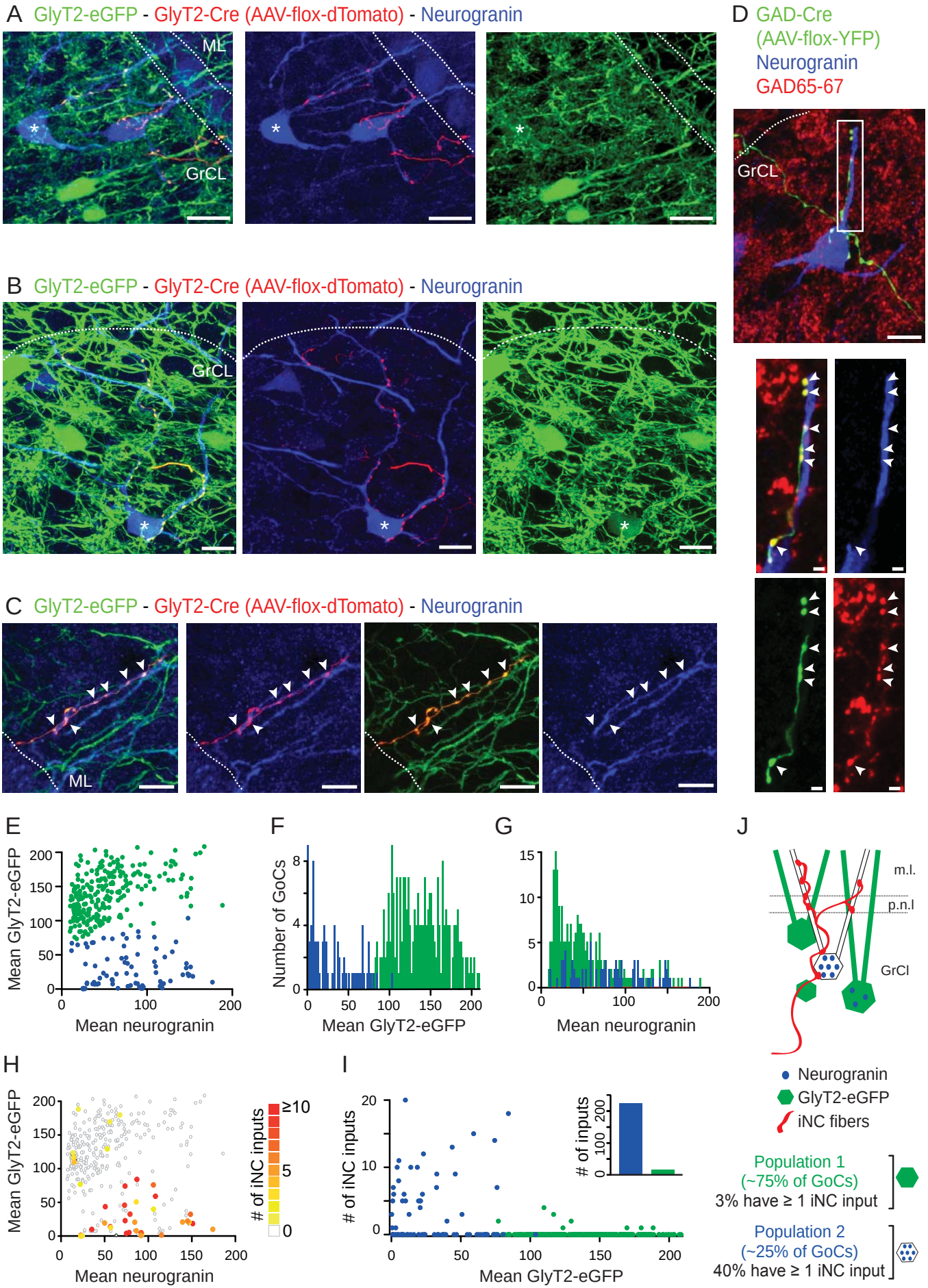

Ankri, Husson et al.
Fig 5

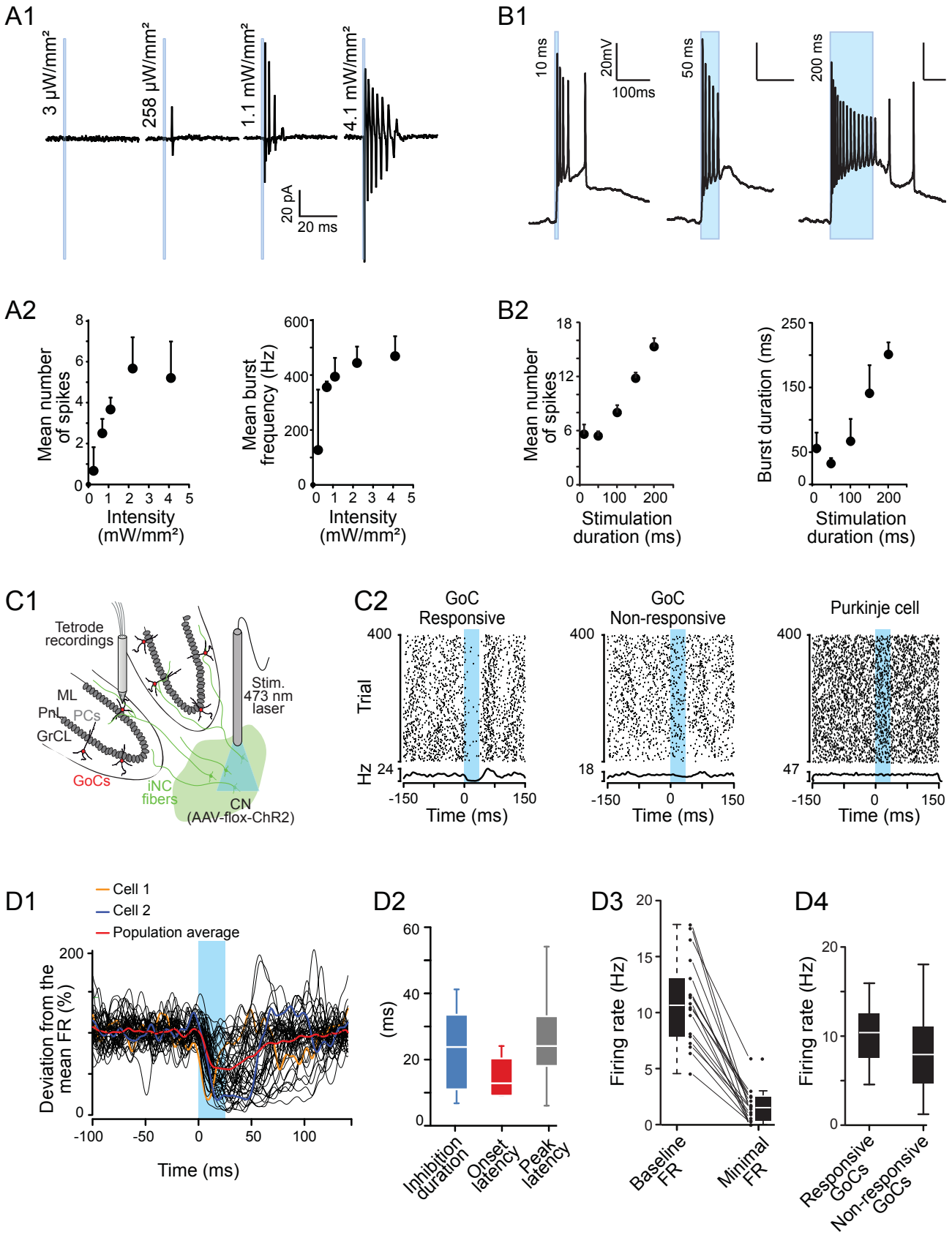

Ankri, Husson et al.
Fig 6